Scientific Report No. 95

BORN-TYPE RECONSTRUCTION OF MATERIAL PARAMETERS OF AN INHOMOGENEOUS, LOSSY DIELECTRIC SLAB FROM REFLECTED-FIELD DATA

Anton G. Tijhuis[1]

Electromagnetics Laboratory
Department of Electrical and Computer Engineering
University of Colorado
Campus Box 425
Boulder, Colorado 80309

December 1987

Also available as Report 1988-02 from:

Laboratory of Electromagnetic Research
Department of Electrical Engineering
Delft University of Technology
P.O. Box 5031, 2600 GA Delft
The Netherlands

[1]Presently on leave from Laboratory of Electromagnetic Research,. Delft University of Technology, The Netherlands.

Abstract

This paper considers several Born-type techniques for reconstructing the permittivity and/or the conductivity profiles of a one-dimensionally inhomogeneous, lossy dielectric slab from reflected-field data. Traditionally, the properties of such techniques have been found mainly by numerical experimentation. In the present paper, a closed-form analysis is given that explains these properties. It is argued that there exists only one version of the Born-type scheme that leads to a fully detailed reconstruction of the unknown profiles. All other versions suffer from an inherent band limitation. Our conclusions are confirmed numerically as well as by using alternative inversion techniques.

Contents

Chapter 1

Introduction

We consider solving the one-dimensional inverse-scattering problem for an inhomogeneous, lossy slab of given thickness embedded in vacuum. In this inverse-profiling problem, the reflected field caused by one or more plane, electromagnetic waves normally incident from one or both sides of the slab is assumed to be known. The aim of the inverse-profiling computation is to reconstruct the conductivity and/or the permittivity of the slab from these reflected-field data. In particular, we consider whether this inverse-profiling problem can be solved by using contrast-source integral representations for these fields.

In order to put our approach into some perspective, we first review the techniques that have been reported in the literature for the solution of the problem specified above and the related one of the slab terminated by a perfectly conducting boundary. In view of the large number of papers on this problem, we will only list related applications from acoustics and elastodynamics when a suitable reference from electromagnetics is not available. In addition, we will disregard all situations where the source is localized.

The problem of a lossless slab was first theoretically treated by Kay [24]. Through a Liouville transformation, he reduced it to an equivalent, uniquely solvable, quantum-mechanical scattering problem. This equivalence also allows the reconstruction of the unknown susceptibility profile through one of the many approaches developed for the quantum-mechanical problem (for reviews, see [6], [7], [37] and [40]). The practical aspects of this approach have, for instance, been discussed in [1], [11]. Numerical results were first reported in [8], [42]. More recent results can be found in [13], [18]–[20] and

[28]. The main difficulty appears to be the Liouville transformation, which involves a double space differentation of the unknown refractive index. Since, for practical applications, we must allow this refractive index to be discontinuous at least at the slab's interfaces, numerical difficulties can be expected in reconstructing the equivalent quantum-mechanical scattering potential, which involves recovering delta functions and their derivatives at *a priori* unknown locations. A second disadvantage of the Liouville transformation is that its typically one-dimensional character prevents, from the outset, any generalization to more complicated geometries.

The generalization of the quantum-mechanical approach to the case of a lossy slab was first tackled by Weston and Krueger [54]–[56]. Their approach, which uses the time-domain reflected fields caused by a delta-function incident pulse, was elaborated by a number of authors. Recently, this has culminated in a series of survey papers by Kristensson and Krueger [25]–[27]. The equivalent frequency-domain problem was analyzed from a theoretical point of view by Jaulent [21], [22]. For this problem, numerical results have not yet been reported. As in the lossless case, the main disadvantage lies in the necessary Liouville transformation. For the time-domain case, problems may also arise in the determination of the delta-function responses, which, in a practical situation, amounts to a deconvolution problem. As is well known (see e.g. [41]), such deconvolution problems are numerically ill posed.

In the geophysical literature, one usually follows an entirely different approach and models the medium by a number of homogeneous layers, all of which have a common one-way travel time [15]. The system is described completely by the set of reflection coefficients at the interfaces between these layers. Surveys of methods for solving these reflection coefficients for lossles media systems, which are the geophysical equivalent of lossless layered dielectric systems, can be found in [5], [34]. An electromagnetic application to an inhomogeneous, lossy medium was carried out by Lee [30]. The principal disadvantage of the approach is that, in the piecewise-homogeneous model, a large number of layers must be taken to arrive at an acceptable description of the reflected fields. Since each layer is associated with one or two unknown material parameters, stability problems are encountered when the scheme is applied to process practical reflected fields caused by band-limited incident pulses.

In the electromagnetic literature we can, in addition to the quantum-mechanical approach, distinguish two trends in developing solution methods

for the one-dimensional inverse-scattering problem. In the first one, integral relations pertaining to the corresponding direct-scattering problem are being used as additional relations between the known reflected-field data and the unknown fields and constitutive parameters inside the slab. In conjunction with the corresponding direct-scattering integral or differential equations, these relations are then used to resolve the inverse-scattering problem.

One way to achieve this objective is to accurately trace the wavefront in the time-domain case (see [3], [4], [12] and [31]). This has the disadvantage that the unknown value of the susceptibility or conductivity is obtained from the numerically computed field at the wavefront, which is afflicted with a large relative error. As a consequence, the method is restricted to pulses with steep ramp-like fronts.

An alternative is the Born-type approximation of making some educated guess about the unknown field inside the slab, and substituting this guess in the additional relations involving the known reflection data. These relations can then be regarded as one or two integral equations of the first kind, whose solution yields an approximation to the unknown permittivity and/or conductivity profiles. The first application along these lines is due to Tabbara ([43], [44]), who used a *single-step* version to reconstruct the unknown permittivity profile of an inhomogeneous, lossles half-space from frequency-domain data. *Iterative procedures* were subsequently applied by a number of authors ([9], [16], [17], [39], [45], [49] and [53]). In such procedures, successive approximations for the unknown field inside the slab and the unknown constitutive parameters are obtained by alternately solving an approximate direct-scattering problem and an approximate inverse-scattering problem.

The second trend in the solution of one-dimensional, electromagnetic inverse-scattering problems is the use of nonlinear optimization techniques. Such techniques are applied to minimize some cost function involving the deviation between the known reflection data and their counterparts in some trial medium characterized by a finite set of parameters. Succesful applications were described in [32], [33], [36] and [38]. The essential difference with the Born-type iterative procedure is not the introduction of a cost function. In fact, the solution of the Born-approximated integral equations for the unknown profiles in each step also involves the minimization of a cost function. Rather, the difference is that the nonlinear optimization techniques are guaranteed to converge, albeit at a considerably slower rate than the less reliable Born-type iterative procedure.

Compared with the quantum-mechanical techniques listed above, both the Born-type scheme and the optimization approach have the advantage that, through the cost function, imperfections in the known reflected-field data can be compensated for by taking into account known *a priori* information about the configuration. Furthermore, they would appear to be generalizable to more complicated scattering geometries. On the other hand, these schemes and their properties have, until now, mainly been determined by numerical experimentation, and, hence, lack the theoretical foundation of the quantum-mechanical approach.

In the present paper, an attempt is made to supply such a foundation for the Born-type scheme. To this end, we formulate the problem in a more rigorous manner, and we analyze the error made in enforcing the Born-type approximation of replacing an unknown field inside the slab by a corresponding known field in some reference configuration. For the case of small contrast, the analysis can be carried through rigorously in closed form. For larger contrasts, we have to revert to WKB expressions for the frequency-domain solutions to the direct-scattering problem of a plane wave incident on an inhomogeneous slab configuration. This approximation seems justified since we expect most of the difficulties with the Born-type scheme at high frequencies, and since the WKB approximations are exact for homogeneous, lossless slabs.

The consequences of our analysis for the numerical implementation of a Born-type scheme coincide with the conclusions previously obtained from numerical experiments. Moreover, a single version of the Born-type iterative procedure can be selected that does not suffer from the inherent limitations experienced in these experiments. This observation is verified numerically, by reconstructing some of the same profiles that were previously recovered by other versions of the iterative procedure.

Finally, the application of optimization and Prony-type techniques to the inverse-profiling problems handled by the improved Born-type iterative scheme provides an independent validation of our analytical and numerical results.

Chapter 2

Formulation of the problem

We consider the scattering of electromagnetic waves by a one-dimensionally inhomogeneous, lossy dielectric slab (Figure 2.1) of thickness d, embedded in vacuum. A Cartesian coordinate system is introduced, with z as the coordinate normal to the boundaries of the slab and x and y as coordinates parallel to them. The configuration consists of three domains $\mathcal{D}_n$ (with $n = 1, 2, 3$), where regions $\mathcal{D}_1$ and $\mathcal{D}_3$ contain vacuum, and region $\mathcal{D}_2$ the dielectric material.

For the incident field, we take one or both of the linearly polarized, electromagnetic pulses

$$\underline{\mathcal{E}}^i_+(\underline{r},t) = \mathcal{E}^i_+(z,t)\underline{i}_y = \mathcal{F}(t - z/c_0)\underline{i}_y, \tag{2.1}$$

$$\underline{\mathcal{H}}^i_+(\underline{r},t) = \mathcal{H}^i_+(z,t)\underline{i}_x = -Y_0\mathcal{F}(t - z/c_0)\underline{i}_x, \tag{2.2}$$

and

$$\underline{\mathcal{E}}^i_-(\underline{r},t) = \mathcal{E}^i_-(z,t)\underline{i}_y = \mathcal{F}(t - (d-z)/c_0)\underline{i}_y, \tag{2.3}$$

$$\underline{\mathcal{H}}^i_-(\underline{r},t) = \mathcal{H}^i_-(z,t)\underline{i}_x = Y_0\mathcal{F}(t - (d-z)/c_0)\underline{i}_x, \tag{2.4}$$

where $Y_0 = \sqrt{\epsilon_0/\mu_0}$, $c_0 = 1/\sqrt{\epsilon_0\mu_0}$ (c_0 is the speed of electromagnetic waves in vacuum). The incident pulse is chosen such that $\mathcal{F}(t)$ vanishes outside the domain $0 < t < T$. The subscripts $+$ and $-$ refer to the direction of propagation.

To each of these fields corresponds a total field, which, in line with the notation used for the incident fields, is written as

$$\underline{\mathcal{E}}_\alpha(\underline{r},t) = \mathcal{E}_\alpha(z,t)\underline{i}_y, \tag{2.5}$$

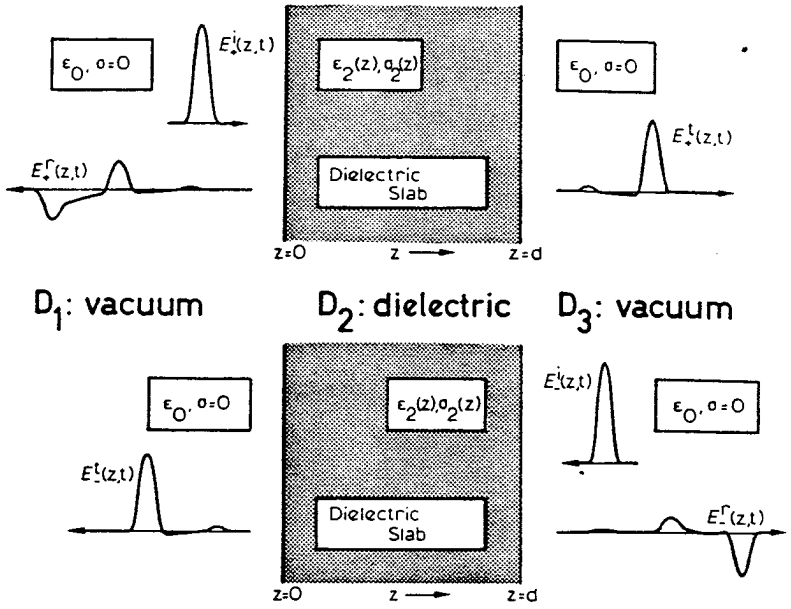

Figure 2.1: Pulsed plane waves normally incident from the left and from the right on an inhomogeneous, lossy dielectric slab embedded in vacuum.

$$\underline{\mathcal{H}}_\alpha(\underline{r},t) = \mathcal{H}_\alpha(z,t)\underline{i}_x, \tag{2.6}$$

where the label α stands for either of the labels $+$ and $-$ that occur as subscripts in the definitions of the incident fields given above.

For $\alpha = +$ and $\alpha = -$, the incident field originates from $\mathcal{D}_1$ and $\mathcal{D}_3$, respectively. These regions will also be referred to as the *region of incidence* $\mathcal{D}_i$. The half-space on the opposite side of the slab will be called the *region of transmission* $\mathcal{D}_t$. Using these definitions, we can identify the reflected and transmitted fields corresponding to the incident fields specified in Equations (2.1)–(2.4) as

$$\mathcal{E}_\alpha^r(z,t) = \mathcal{E}_\alpha(z,t) - \mathcal{E}_\alpha^i(z,t) \quad \text{in } \mathcal{D}_i, \tag{2.7}$$

$$\mathcal{E}_\alpha^t(z,t) = \mathcal{E}_\alpha(z,t) \quad \text{in } \mathcal{D}_t. \tag{2.8}$$

For the reflected field, we have the relations

$$\mathcal{E}_\alpha^r(z,t) = \mathcal{E}_\alpha^r(z_\alpha, t - \mid z - z_\alpha \mid /c_0) \text{ in } \mathcal{D}_i, \tag{2.9}$$

with $\alpha = \pm$, where z_α is the coordinate of the interface of the slab with the region of incidence, i.e. $z_+ = 0$ and $z_- = d$. Similar relations hold for the transmitted field.

In addition to the time-domain fields specified above, we will, in the present discussion, also consider the Laplace transforms of these electromagnetic field quantities, e.g.

$$E_\alpha(z,s) \stackrel{\text{def}}{=} \int_{-\infty}^{\infty} \exp(-st)\mathcal{E}_\alpha(z,t)\,dt. \tag{2.10}$$

Since the incident field reaches the slab at $t = 0$, the time-domain signals are causal, and the Laplace transforms are regular for Re(s) ≥ 0. These Laplace transforms are related to the conventional, unit-amplitude frequency-domain solutions $\hat{E}_\alpha(z,s)$ (with $\alpha = \pm$) via the equality

$$E_\alpha(z,s) = F(s)\hat{E}_\alpha(z,s), \tag{2.11}$$

where

$$F(s) = \int_0^T \mathcal{F}(t)\exp(-st)\,dt \tag{2.12}$$

denotes the Laplace transform of the incident field. Outside the slab, the normalized solutions $\hat{E}_\alpha(z,s)$ can be written in the form

$$\hat{E}_+(z,s) = \begin{cases} \exp(-sz/c_0) + r^+(s)\exp(sz/c_0) & \text{in } \mathcal{D}_1, \\ t^+(s)\exp(-s(z-d)/c_0) & \text{in } \mathcal{D}_3, \end{cases} \tag{2.13}$$

and

$$\hat{E}_-(z,s) = \begin{cases} t^-(s)\exp(sz/c_0) & \text{in } \mathcal{D}_1, \\ \exp(s(z-d)/c_0) + r^-(s)\exp(-s(z-d)/c_0) & \text{in } \mathcal{D}_3, \end{cases} \tag{2.14}$$

with $r^\alpha(s)$ and $t^\alpha(s)$ being the reflection and transmission coefficients, respectively. These unit-amplitude plane waves are illustrated graphically in Figure 2.2. The first line of Equation (2.13) and the second line of Equation (2.14) are the frequency-domain counterparts of the time-domain relation given in Equation (2.9).

In this paper, we consider solving the inverse-scattering problem for the configuration defined above. In this so-called *inverse-profiling* problem, the reflected field caused by one or more plane, electromagnetic waves incident from one or both sides if the slab is assumed to be known. The aim of the inverse-profiling computation is to reconstruct one or both of the material parameters of the slab, i.e. the permittivity $\epsilon(z)$ and the conductivity $\sigma(z)$, from these reflected-field data. In particular, we investigate whether

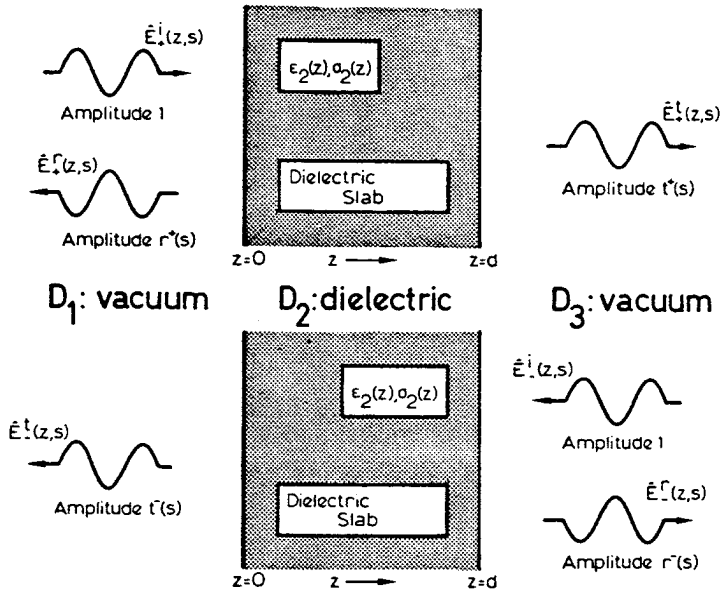

Figure 2.2: Monochromatic plane waves normally incident from the left and from the right on an inhomogeneous, lossy dielectric slab embedded in vacuum.

the inverse-scattering problem can be resolved by utilizing integral relations for these reflected fields. We will consider both the frequency-domain case, where the reflection coefficient for plane-wave incidence, as introduced in Equations (2.13), (2.14), is known for a specified range of real frequencies ($s = i\omega$), and the time-domain case, where the known data consists of the (sampled) reflected field caused by an incident pulse of finite duration T. As can be observed from Equations (2.9), (2.13), (2.14), it suffices in both cases to consider the reflected fields at the slab's boundaries; field data recorded at other observation points outside the slab can be reduced directly to equivalent fields at these boundaries.

In explaining the algorithm, we will mainly consider the case of "ideal" reflected-field data. This will allow us to demonstrate the analytical as well as the numerical aspects of the algorithm in full detail. On the other hand, we want our analysis to be as "realistic" as is possible for a one-dimensional problem. Therefore, we will also devote attention to the case where the reflected-field data suffer from high-frequency band limitations, and from noise.

Chapter 3

Integral relations

Before we formulate the actual inversion procedure, we review, in this chapter, the basic integral relations that we can utilize in such a procedure. To simplify the notation, we introduce a set of dimensionless quantities that are more natural to the problem at hand. First, we normalize all distances with respect to the slab thickness d, and all times with respect to the vacuum travel time across the slab, i.e. d/c_0; e.g.

$$\breve{z} = z/d, \quad \breve{t} = c_0 t/d. \tag{3.1}$$

Second, we introduce the dimensionless quantities

$$\breve{s} = sd/c_0, \quad \breve{\sigma}(\breve{z}) = Z_0\sigma(z)d, \quad \breve{\epsilon}_r(\breve{z}) = \epsilon_r(z). \tag{3.2}$$

Third, we introduce the normalized field quantities

$$\breve{E}(\breve{z},\breve{s}) = E(z,s), \quad \breve{H}(\breve{z},\breve{s}) = Z_0 H(z,s), \tag{3.3}$$

where $Z_0 = \sqrt{\mu_0/\epsilon_0}$, and where $\epsilon_r(z) = \epsilon(z)/\epsilon_0$ denotes the relative permittivity. In further discussion, we will use these normalized quantities, omitting the breves.

The transformed, normalized, source-free electromagnetic field equations are then given by

$$\partial_z H(z,s) = s(\epsilon_r(z) + \sigma(z)/s)E(z,s), \tag{3.4}$$

$$\partial_z E(z,s) = sH(z,s). \tag{3.5}$$

Elimination of H leads to

$$[\partial_z^2 - s^2(\epsilon_r(z) + \sigma(z)/s)]E(z,s) = 0, \tag{3.6}$$

which will be regarded as our fundamental differential equation.

In order to arrive at the desired contrast-source integral relations, we now introduce a *background medium* with *known* constitutive coefficients $\tilde{\epsilon}_r(z)$ and $\tilde{\sigma}(z)$, and $\tilde{E}_\alpha(z,s)$ as the corresponding unit-amplitude solutions in the background configuration, normalized according to Equations (2.13), (2.14). Further, we introduce the Green's function of the background medium as being the solution of

$$[\partial_z^2 - s^2\tilde{\epsilon}_r(z) - s\tilde{\sigma}(z)]\tilde{G}(z,z';s) = -\delta(z-z'), \tag{3.7}$$

which satisfies the radiation condition as $\mid z \mid \rightarrow \infty$. The solutions $\tilde{E}_\alpha(z,s)$ for $\alpha = \pm$ are essentially the same as the *Jost solutions* used in quantum scattering theory (see [7]). Accordingly, we can write the Green's function of the background medium as the product

$$\tilde{G}(z,z';s) = \tilde{E}_+(z_>,s)\tilde{E}_-(z_<,s)/W(\tilde{E}_-,\tilde{E}_+), \tag{3.8}$$

where $W(\tilde{E}_-,\tilde{E}_+)$ denotes the Wronskian

$$\begin{aligned} W(\tilde{E}_-,\tilde{E}_+) &= \tilde{E}_+(z,s)\partial_z\tilde{E}_-(z,s) - \tilde{E}_-(z,s)\partial_z\tilde{E}_+(z,s) \\ &= 2s\tilde{t}^-(s) = 2s\tilde{t}^+(s). \end{aligned} \tag{3.9}$$

Equation (3.9) provides us with an interesting side result: the transmission coefficients for incidence from both sides of the slab are identical. Hence, each of these coefficients must contain the same information about the slab configuration. As a consequence, it would be superfluous to measure more than one of them. A numerical confirmation of this result can be obtained from the transient fields shown in Figure 2.1, which have been computed by applying the marching-on-in-time method as described in [45] and [46, Section 3.3] to the scattering of sine-squared incident pulses by an asymmetric, inhomogeneous, lossy slab. Clearly, the transmitted fields displayed in this figure are identical. A similar result can be derived for the case where the slab is embedded between two homogeneous dielectric half-spaces.

To arrive at the integral relation, we now rewrite the second-order differential equation (3.6) as

$$[\partial_z^2 + s^2(\tilde{\epsilon}_r(z) + \tilde{\sigma}(z)/s)]E(z,s) = s^2\tilde{C}(z,s)E(z,s), \tag{3.10}$$

where the *contrast function* $\tilde{C}(z,s)$ is defined as

$$\tilde{C}(z,s) \stackrel{\text{def}}{=} \epsilon_r(z) - \tilde{\epsilon}_r(z) + [\sigma(z) - \tilde{\sigma}(z)]/s. \tag{3.11}$$

Interpreting the right-hand side of the rewritten equation as a contrast source, and applying the superposition principle, we can then directly combine Equations (3.7) and (3.10) into

$$\hat{E}_\alpha(z,s) = \tilde{E}_\alpha(z,s) - s^2 \int_{-\infty}^{\infty} \tilde{G}(z,z';s)\tilde{C}(z',s)\hat{E}_\alpha(z',s)\,dz'. \tag{3.12}$$

It should be stressed that, in this integral relation, the background medium inside the slab can, in principle, still be given by any arbitrary combination of the constitutive parameters $\{\tilde{\epsilon}_r(z), \tilde{\sigma}(z)\}$. In this respect, Equation (3.12) can be regarded as representing an infinite class of integral relations.

The integral relation (3.12) assumes a special form when we take $z = z_\alpha$, with z_α as defined in connection with Equation (2.9). Using the identities

$$\tilde{E}_+(1,s) = \tilde{t}^+(s) \quad , \quad \tilde{E}_-(0,s) = \tilde{t}^-(s), \tag{3.13}$$

which follow directly from Equations (2.13), (2.14), we obtain

$$\begin{aligned} r^\alpha(s) - \tilde{r}^\alpha(s) &= \hat{E}_\alpha(z_\alpha,s) - \tilde{E}_\alpha(z_\alpha,s) \\ &= -\frac{s}{2}\int_0^1 \tilde{C}(z,s)\tilde{E}_\alpha(z,s)\hat{E}_\alpha(z,s)\,dz, \end{aligned} \tag{3.14}$$

with $\alpha = \pm$. The pair of equations given in (3.14) can also be envisaged as a pair of *reciprocity relations* between the fields $\hat{E}_\alpha(z,s)$ and $\tilde{E}_\alpha(z,s)$ (see [2]).

Of special interest in our analysis will be the case where the background medium is a vacuum. In that case, we directly have $\tilde{E}_\alpha(z,s) = \hat{E}^i_\alpha(z,s)$, with $\hat{E}^i_\alpha(z,s)$ being unit-amplitude incident fields normalized in accordance with Equations (2.13), (2.14). These fields are given by

$$\hat{E}^i_+(z,s) \stackrel{\text{def}}{=} \exp(-sz), \tag{3.15}$$

$$\hat{E}^i_-(z,s) \stackrel{\text{def}}{=} \exp(-s(1-z)). \tag{3.16}$$

Substituting the expressions given in (3.15), (3.16) into Equations (3.8), (3.9), and (3.13) yields the conventional free-space Green's function

$$G_0(z,z';s) = (2s)^{-1}\exp(-s \mid z - z' \mid). \tag{3.17}$$

Combining Equations (3.11), (3.12), and (3.17) then leads to the integral relation

$$\hat{E}_\alpha(z,s) = \hat{E}^i_\alpha(z,s) - s^2 \int_0^1 G_0(z,z';s) C_0(z',s) \hat{E}_\alpha(z',s)\, dz', \tag{3.18}$$

where

$$C_0(z,s) = \chi(z) - \sigma(z)/s \tag{3.19}$$

denotes the contrast function with respect to free space. In (3.19), $\chi(z) \stackrel{\text{def}}{=} \epsilon_r(z) - 1$ denotes the dielectric susceptibility.

The main advantage of Equation (3.18) over the general form (3.12) is that, in the former, the Green's function is known in closed form. This explains why this particular version is commonly used in integral-equation approaches to solving the direct-scattering problem of determining one or both of the fields $\hat{E}_\alpha(z,s)$.

Finally, combining Equations (2.13), (2.14), and (3.14)–(3.16) leads to the integral relations for the reflected field

$$r^\alpha(s) = -\frac{s}{2} \int_0^1 C_0(z,s) \hat{E}^i_\alpha(z,s) \hat{E}_\alpha(z,s)\, dz, \tag{3.20}$$

which have a similar advantage over the general form (3.14).

With Equations (3.12), (3.14), (3.18) and (3.20), we are now in a position to formulate and analyze the various versions of the Born-type inversion procedure.

Chapter 4

Method of solution

The method by which we solve the inverse-scattering problem formulated in Chapter 2 is based on the observation that, for known values of the material parameters $\epsilon_r(z)$ and $\sigma(z)$, the electric fields $\hat{E}_\alpha(z,s)$ can either be solved from the pair of equations (3.4), (3.5), or from any one of the equations (3.6), (3.12), and (3.18). On the other hand, for known values of the reflection coefficients $r^\alpha(s)$ and the unit-amplitude fields $\hat{E}_\alpha(z,s)$, both Equations (3.14) and (3.20), with $\alpha = \pm$, can be envisaged as a pair of integral equations of the first kind for the constitutive coefficients $\epsilon_r(z)$ and $\sigma(z)$. This suggests that it may be possible to determine both the unknown fields $\hat{E}_\alpha(z,s)$ and the unknown "profile(s)" $\epsilon_r(z)$ and/or $\sigma(z)$ by utilizing equations of either type. In particular, we aim at an inversion procedure that generates a single or successive approximations to these unknown quantities.

4.1 The Born-type approximation

The fundamental step in our method of solution is the so-called *Born-type approximation.* In this approximation, we introduce a known *reference medium* with constitutive coefficients $\overline{\epsilon}_r(z)$ and $\overline{\sigma}(z)$. This reference medium should be the best available guess for the actual configuration. Further, we define the fields $\overline{E}_\alpha(z,s)$ as the unit-amplitude solutions in the reference configuration. By considering the reference medium as one special choice of the background medium as discussed in Chapter 3, we then directly have the

integral relation

$$\hat{E}_\alpha(z,s) = \overline{E}_\alpha(z,s) - s^2 \int_0^1 \overline{G}(z,z';s)\overline{C}(z',s)\hat{E}_\alpha(z',s)\,dz', \tag{4.1}$$

where the Green's function $\overline{G}(z,z';s)$ and the contrast function $\overline{C}(z,s)$ are found by substituting $\bar{\epsilon}_r(z)$, $\overline{\sigma}(z)$, and $\overline{E}_\alpha(z,s)$ in (3.8) and (3.11).

Substituting this relation in the "additional" relation (3.14) yields

$$r^\alpha(s) - \tilde{r}^\alpha(s) = -\frac{s}{2}\int_0^1 \tilde{C}(z,s)\tilde{E}_\alpha(z,s)\overline{E}_\alpha(z,s)\,dz + \Delta r_B^\alpha(s), \tag{4.2}$$

where the *Born error* $\Delta r_B^\alpha(s)$ is given by

$$\Delta r_B^\alpha(s) \stackrel{\text{def}}{=} \frac{s^3}{2}\int_0^1 \tilde{C}(z,s)\tilde{E}_\alpha(z,s)\int_0^1 \overline{G}(z,z';s)\overline{C}(z',s)\hat{E}_\alpha(z',s)\,dz'\,dz. \tag{4.3}$$

Now, the *Born-type approximation* consists of neglecting the *Born error* $\Delta r_B^\alpha(s)$ in Equation (4.2). Making this approximation reduces (4.2), with $\alpha = \pm$, to a system of approximate integral equations of the first kind for the unknown profiles $\epsilon_r(z)$ (or, equivalently, $\chi(z)$), and $\sigma(z)$. Note that Equations (4.2) and (4.3) still hold rigorously for any choice of the background medium $\{\tilde{\epsilon}_r(z), \tilde{\sigma}(z)\}$.

Obviously, we could also have obtained the Born-approximated integral equations for the unknown profiles by directly replacing the unknown fields $\hat{E}_\alpha(z,s)$ with the corresponding reference solutions $\overline{E}_\alpha(z,s)$. However, the present approach offers the advantage that we end up with an expression for the approximation error. Even though this expression contains the unknown actual field inside the slab, its magnitude can be estimated. In fact, it is this estimate which, in Chapter 6, will eventually decide which version of the Born-type scheme produces the "best possible" reconstruction.

4.2 Born-type inversion procedures

When the Born error $\Delta r_B^\alpha(s)$ is set to zero in Equation (4.2), the equality sign in that equation no longer holds exactly. Hence, we must determine the unknown profile(s) $\epsilon_r(z)$ and/or $\sigma(z)$ by minimizing an integrated squared error of the form

$$\sum_\alpha \int_{-\infty}^{\infty} w^2(\omega)\left|r^\alpha(i\omega) + \frac{i\omega}{2}\int_0^1 \tilde{C}(z,i\omega)\tilde{E}_\alpha(z,i\omega)\overline{E}_\alpha(z,i\omega)\,dz\right|^2 d\omega, \tag{4.4}$$

where α runs over one or both of the labels $+$ and $-$, and where $w(\omega)$ is a real-valued weighting function. This weighting function can, for example, be identified as the magnitude of the Laplace-transformed incident-pulse shape $F(i\omega)$ (see also Equation (2.11)). In addition, it can be used to account for possible band limitations in the measured reflected-field data. The approximated profiles $\epsilon_{rB}(z)$ and $\sigma_B(z)$ found from minimizing (4.4) are usually referred to as *distorted-wave Born approximations* [10].

As remarked in the introduction, we can basically distinguish two ways of incorporating the Born-type approximation formulated above in an inversion procedure. In the first place, we can perform the inversion in a *single step.* This procedure is particularly appropriate when it is known from *a priori* information that the contrast in material parameters with the surrounding vacuum is small. This case will be discussed in more detail in Chapter 5. For larger contrasts, the results obtained must be subjected to a suitable correction procedure. Examples of such correction procedures can be found in [19], [43], [44] and [46, Subsection 5.4.2]. A brief discussion of the last example will also be given in Section 7.1.

In the second place, we can incorporate the Born-type approximation in an *iterative scheme* that leads to successive approximations for the unknown total field(s) as well as for the unknown constitutive parameter(s). In that case, we start from some initial guess, and we take, in each iteration step, the reference medium identical to the approximation obtained previously. Different versions of this scheme will be discussed in Chapter 6.

4.3 Implicit assumptions

In the above formulation of Born-type inversion procedures, we have made three implicit assumptions that need to be justified for each particular version of the scheme.

The first two pertain to the equations obtained by neglecting the Born error $\Delta r_B^\alpha(s)$ in Equation (4.2). The first one is that these equations suffice for the unique determination of an approximate configuration, at least within some limitations. The second assumption is that the Born error is small enough for this approximation to be a better estimate than the reference medium. Only by justifying both assumptions can we show that a Born-type approach is feasible. In the upcoming two chapters, we will analyze these assumptions and their consequences for the numerical implementation for

various versions of the procedure.

In doing so, we will run up against the problem of selecting the most suitable background medium. At first glance, there seems to be some advantage in selecting a vacuum. Free-space Green's functions are known in closed form in both the time domain and the frequency domain in both one- and multi-dimensional problems. Hence, selecting a vacuum keeps open the possibility of generalizing the method to more complicated inverse-scattering problems. In addition, we have the practical advantage that the discretization of the relevant integral equation may be available from the solution of the corresponding direct-scattering problem. On the other hand, it is by no means clear whether the selection of a vacuum background medium produces the most accurate approximation of the unknown slab configuration. In fact, it will be shown in Chapter 6 that this third implicit assumption is generally not justified.

Chapter 5

The case of small contrast

The most simple example of an application of the method of solution discussed in Chapter 4 is the reconstruction of a small susceptibility $\chi(z)$ and a small conductivity $\sigma(z)$ from the known real-frequency behavior of the reflection coefficient for both directions of incidence. For this particular problem, is seems natural to choose both the reference medium and the background medium to be a vacuum, and to perform the inversion in a single step. In fact, this is the "classical" Born approximation.

This small-contrast problem can also be regarded as the most simple example of a step in the iterative scheme. Hence, it constitutes an ideal starting point for gaining insight into the type of results and difficulties that we can expect in analyzing and implementing a Born-type procedure.

5.1 The Born approximation

As remarked above, the Born approximation can be phrased as neglecting the difference between the actual reflection coefficients $r^\alpha(s)$ and their appropriate counterparts obtained by replacing, in (3.20), the unknown plane-wave responses $\hat{E}_\alpha(z,s)$ by the known incident fields $\hat{E}^i_\alpha(z,s)$. This approximate reflection coefficient can be expressed as

$$r^\alpha_B(s) \stackrel{\text{def}}{=} -\frac{s}{2}\int_0^1 C_0(z,s)\hat{E}^i_\alpha(z,s)^2\,dz. \tag{5.1}$$

With the definitions of the unit-amplitude fields $\hat{E}^i_\alpha(z,s)$ given in (3.15), (3.16), the right-hand side of Equation (5.1) can be recognized as a Laplace

transform. This allows us to derive closed-form expressions for the unknown profiles $\chi(z)$ and $\sigma(z)$. Let the spatial Fourier transforms of these profiles be given by

$$\hat{\chi}(k) \stackrel{\text{def}}{=} \int_{-\infty}^{\infty} \exp(-ikz)\chi(z)\,dz, \tag{5.2}$$

$$\hat{\sigma}(k) \stackrel{\text{def}}{=} \int_{-\infty}^{\infty} \exp(-ikz)\sigma(z)\,dz. \tag{5.3}$$

Then, with the definition of $C_0(z,s)$ given in (3.19), we directly obtain

$$\hat{\chi}(k) = \frac{2i}{k}[r_B^+(\frac{ik}{2}) - \exp(-ik)r_B^-(-\frac{ik}{2})], \tag{5.4}$$

$$\hat{\sigma}(k) = -r_B^+(\frac{ik}{2}) - \exp(-ik)r_B^-(-\frac{ik}{2}). \tag{5.5}$$

Although Equations (5.4), (5.5) hold rigorously for known values of the Born-approximated reflection coefficients $r_B^\alpha(s)$, they only lead to an approximate solution of the inverse-scattering problem, where the actual reflection coefficients $r^\alpha(s)$ are known instead. Hence, we must replace former by the latter in (5.4), (5.5). This results in the Born-approximated Fourier coefficients

$$\hat{\chi}_B(k) = \frac{2i}{k}[r^+(\frac{ik}{2}) - \exp(-ik)r^-(-\frac{ik}{2})], \tag{5.6}$$

$$\hat{\sigma}_B(k) = -r^+(\frac{ik}{2}) - \exp(-ik)r^-(-\frac{ik}{2}), \tag{5.7}$$

where the subscript B has been appended in line with the notation used for the reflection coefficients. Obviously, the approximate susceptibility and conductivity profiles are then defined via the inverse Fourier transformations

$$\chi_B(z) = (2\pi)^{-1}\int_{-\infty}^{\infty} \exp(ikz)\hat{\chi}_B(k)dk, \tag{5.8}$$

$$\sigma_B(z) = (2\pi)^{-1}\int_{-\infty}^{\infty} \exp(ikz)\hat{\sigma}_B(k)dk. \tag{5.9}$$

As remarked in Section 4.1, the error in the results obtained with the aid of these formulas is generated by the deviation between the exact reflection coefficients $r^\alpha(s)$ and their Born approximations $r_B^\alpha(s)$. This error can be estimated by substituting the relevant free-space expressions in the right-hand side of (4.3), and by approximating the unknown total fields $\hat{E}_\alpha(z',s)$

by the corresponding incident fields $\hat{E}^i_\alpha(z',s)$. This results in

$$\Delta r^\alpha_B(s) \approx \frac{s^3}{2}\int_0^1 C_0(z,s)\hat{E}^i_\alpha(z,s)\int_0^1 G_0(z,z';s)C_0(z',s)\hat{E}^i_\alpha(z',s)\,dz'\,dz. \tag{5.10}$$

From Equations (5.4)–(5.9), it is observed that we only need to estimate the right-hand side of (5.10) for $s = i\omega$, with ω being a conventional, real-valued frequency. In that case, the right-hand side can readily be identified as a sum of single and double Fourier integrals, whose magnitude follows from standard Fourier theory (see e.g. [51]).

Assuming that the unknown contrasts $\chi(z)$ and $\sigma(z)$ are of the same order of magnitude, and that $\chi(z)$ exhibits at least one discontinuity in the interval $-\infty < z < \infty$, we find

$$\Delta r^\alpha_B(i\omega) = \begin{cases} \mathcal{O}(\chi^2) & \text{for } |\,\omega\,| = \mathcal{O}(1), \\ \omega\mathcal{O}(\chi^2) & \text{as } |\,\omega\,| \to \infty. \end{cases} \tag{5.11}$$

With the aid of this estimate, we can now determine the size of the error in the approximate Fourier coefficients $\hat{\chi}_B(k)$ and $\hat{\sigma}_B(k)$. For $\hat{\chi}_B(k)$, this is achieved by substracting (5.6) from (5.4), and substituting (5.11) and the identity $s = i\omega = \pm ik/2$, which we encountered in all of the equations (5.4)–(5.9). For $\hat{\sigma}_B(k)$, we follow the same procedure, starting from (5.5) and (5.7). We end up with

$$\hat{\chi}(k) - \hat{\chi}_B(k) = \mathcal{O}(\chi^2), \tag{5.12}$$

$$\hat{\sigma}(k) - \hat{\sigma}_B(k) = k\mathcal{O}(\chi^2), \tag{5.13}$$

for $-\infty < k < \infty$.

From the results listed in Equations (5.6)–(5.9) and (5.12), (5.13), some preliminary conclusions can already be drawn about the validity of the implicit assumptions listed in Section 4.3. In the first place, it is observed from (5.6)–(5.9) that, for a complete determination of $\chi_B(z)$ *and* $\sigma_B(z)$, we need to know the real-frequency behavior of *both* reflection coefficients over the *entire* interval $-\infty < \omega < \infty$. By a similar argument, it can be shown that a *single* unknown profile can be reconstructed from the frequency behavior of *one* of these coefficients, provided that the remaining profile is known. In both cases, any band limitation in the known reflected-field data will correspond with a band limitation in the spectral representation of the unknown profile(s).

In the second place, as (5.12), (5.13) show, the error in $\hat{\chi}_B(k)$ remains approximately constant in magnitude over the entire range of k. The error in $\hat{\sigma}_B(k)$, on the other hand, increases linearly in magnitude with increasing $| k |$. Now, the actual Fourier coefficients $\hat{\chi}(k)$ and $\hat{\sigma}(k)$ as defined in (5.2), (5.3), are of $\mathcal{O}(k^{-1})$ as $| k | \to \infty$. Consequently, the approximate inversion formulas (5.6)–(5.9) can at best produce a band-limited reconstruction of the unknown profiles $\chi(z)$ and $\sigma(z)$, even when wide-band reflected-field information is available. In particular, the short-range variation of $\sigma(z)$ will be recovered poorly. Since the small-contrast problem can be regarded as one example of a Born-type iteration step, similar results should be expected for the general, iterative procedure.

5.2 Verification of the conclusions

Independent confirmation of the conclusions stated above can be obtained in two ways. In the first place, the Born-approximated reflection coefficients $r_B^\alpha(s)$ and the estimated Born error $\Delta r_B^\alpha(s)$, as given in (5.1), (5.10), can be interpreted in the context of a *Neumann-series* approach to solving the unit-amplitude fields $\hat{E}_\alpha(z,s)$ from the integral equation that results from (3.18), when z is confined to the interval $0 < z < 1$.

In this approach, we formally write the unknown fields $\hat{E}_\alpha(z,s)$ as a perturbation series of the form

$$\hat{E}_\alpha(z,s) = \hat{E}_\alpha^i(z,s) + \sum_{n=1}^{\infty} \hat{E}_\alpha^{(n)}(z,s), \tag{5.14}$$

where $\hat{E}_\alpha^{(n)}(z,s)$ is assumed to be "n-th order small" (see [23], [52]). Substituting (5.14) in (3.18), and enforcing the equality sign for each order of magnitude separately result in the hierarchy of equations

$$\hat{E}_\alpha^{(n)}(z,s) = -s^2 \int_0^1 G_0(z,z';s) C_0(z',s) \hat{E}_\alpha^{(n-1)}(z',s)\, dz', \tag{5.15}$$

with $n = 1, 2, \ldots, \infty$, and with $\hat{E}_\alpha^{(0)}(z,s) \stackrel{\text{def}}{=} \hat{E}_\alpha^i(z,s)$. Note that the implementation of this approach involves nothing but a repeated evaluation of the Fourier-type integral on the right-hand side of Equation (5.15).

In the context of this approach, $r_B^\alpha(s)$ and the estimate of $\Delta r_B^\alpha(s)$ as given in (5.1), (5.10) are exactly the first- and second-order contributions to the,

now unknown, reflection coefficients $r^{\alpha}(s)$. The band limitation inherent in the Born approximation can then be attributed to the feature that the Neumann-series approach converges only for a small enough $|\, s \,|$ (see [52]).

A second confirmation of the conclusions stated above can be obtained by numerically implementing the approximate inversion procedure as specified in (5.6)-(5.9). In our numerical experiments, we evaluated the integrals in (5.8), (5.9) over some finite interval $-k_{max} < k < k_{max}$ by applying a $(2K + 1)$ times repeated four-point Gauss-Legendre quadrature rule. Details can be found in [46, Subsection 5.3.3]. In particular, we considered the reconstruction of the susceptibility and the conductivity of a homogeneous, lossy dielectric slab. For this configuration, the reflection coefficients $r^{\alpha}(s)$ are available in closed form (see [46, Section 2.2], [47]). Hence, their values are available up to machine precision, and any errors in the reconstructions obtained can be attributed to the Born errors listed in (5.12), (5.13), and to the truncation of the spectral integrals. Some representative results are shown in Figures 5.1 and 5.2. From left to right, Figure 5.1 shows results for $k_{max} = 30, 60, 90$, and $K = 6, 12, 18$, respectively. In the upper half of the figure, the reconstructed susceptibility profile is compared with the actual one. Apparently, the reconstruction is accurate, apart from a local oscillation near the discontinuities, which is simply caused by Gibbs' phenomenon. In the lower half of Figure 5.1, the comparison is repeated for the conductivity profile. Now, the amplitude of the unwanted oscillation increases with increasing k_{max}. Clearly, this increase is caused by the increase in error in $\hat{\sigma}_B(k)$ for large k, as predicted in (5.13).

An even more definite confirmation of the error estimates in (5.12), (5.13) is obtained in Figure 5.2, which compares the sampled values of $\hat{\chi}_B(k)$ and $\hat{\sigma}_B(k)$ that were used in the numerical evaluation of the truncated spectral integrals for $k_{max} = 30$ and $K = 6$ with the corresponding actual Fourier coefficients $\hat{\chi}(k)$ and $\hat{\sigma}(k)$ as defined in (5.2), (5.3). Clearly the results are in agreement with (5.12), (5.13).

Similar numerical experiments were performed for larger contrasts, for inhomogeneous slab configurations, and for oblique incidence. It turns out that the Born approximation provides a reliable reconstruction for contrasts up to $\chi = 0.2$ and $\sigma = 0.1$, and at least a global impression of the configuration for contrasts up to $\chi = 2$ and $\sigma = 1$. This is in agreement with a similar observation by Ge [12], who considered the Born reconstruction of $\sigma(z)$ from single-sided time-domain data in the case where $\chi(z) = 0$. For in-

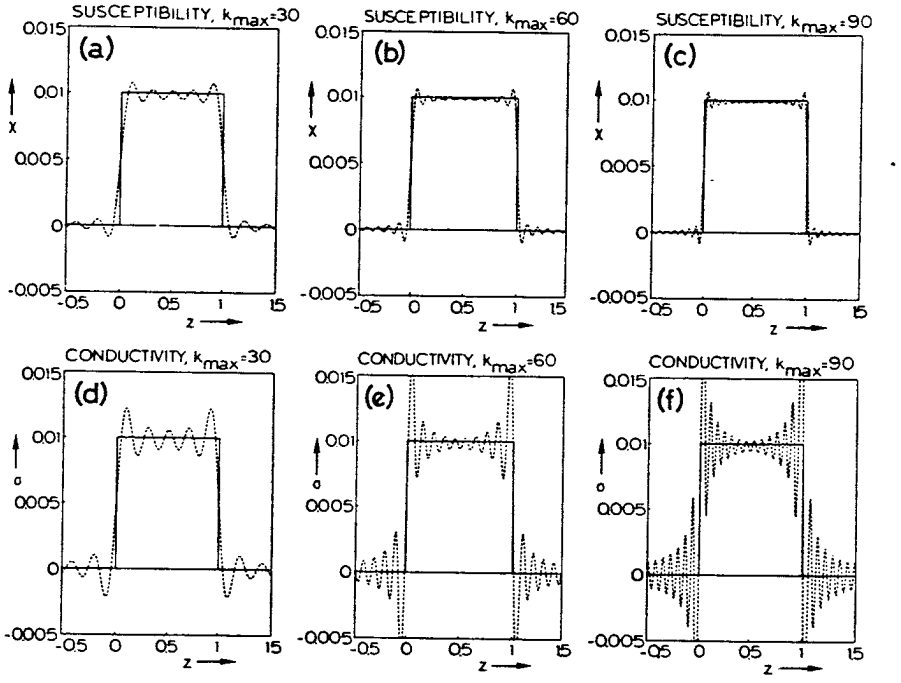

Figure 5.1: Results of the simultaneous Born reconstruction of both $\chi(z) = \sigma(z) = 0.01$ from the reflection coefficients at normal incidence.

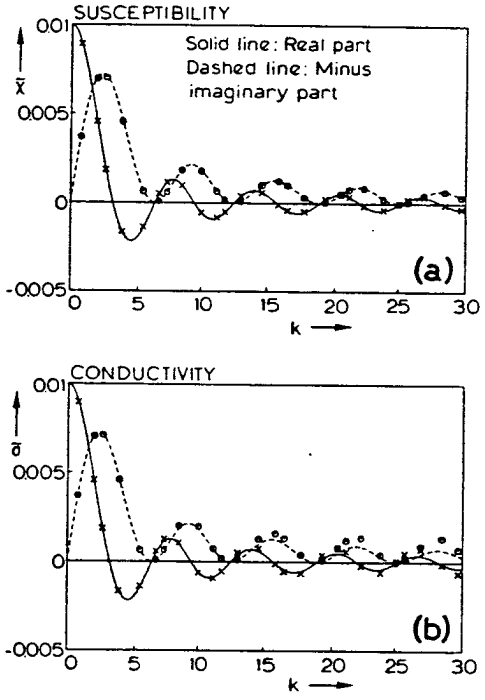

Figure 5.2: Sampled Born approximations $\hat{\chi}_B(k)$ and $\hat{\sigma}_B(k)$ as used in the computations leading to Figures 5.1a,d compared with the actual spatial Fourier transforms $\hat{\chi}(k)$ and $\hat{\sigma}(k)$.

homogeneous slab configurations, the values of the reflection coefficients were computed by numerically integrating the system of equations (3.4), (3.5) with the aid of a fifth- and sixth-order Runge-Kutta-Verner method, as outlined in [46, Subsection 2.4.2], [48], and [49]. A result will be encountered in the next section. For a discussion of the case of oblique incidence, the reader is referred to [46, Section 5.3].

5.3 A numerical inversion procedure

The most annoying disadvantage of the estimation procedure described in the previous two sections is that the agreement between the reconstructed and the actual profiles is confined to a limited range of the spatial wave number k. One way to remedy this situation is to supply additional *a priori* information about the short-range behavior of the unknown profiles. When these profiles are continuous within the slab, this can be achieved by representing them by piecewise-linear expansions of the type

$$\chi(z) = \sum_{m=0}^{M} \chi_m \phi_m(z), \tag{5.16}$$

$$\sigma(z) = \sum_{m=0}^{M} \sigma_m \phi_m(z), \tag{5.17}$$

with the $\{\phi_m(z)\}$ being triangular expansion functions, given by

$$\phi_m(z) \stackrel{\text{def}}{=} \begin{cases} 0 & \text{for } -\infty < z \leq (m-1)/M, \\ 1 - M \mid z - m/M \mid & \text{for } (m-1)/M \leq z \leq (m+1)/M, \\ 0 & \text{for } (m+1)/M \leq z < \infty, \end{cases} \tag{5.18}$$

for $0 < m < M$, and by versions truncated at the slab's interfaces for $m = 0, M$. In (5.16), (5.17) the expansion coefficients $\{\chi_m\}$ and $\{\sigma_m\}$ can be interpreted as being approximations to values of the corresponding profiles $\chi(z)$ and $\sigma(z)$ at $z = m/M$. Compared with global representations such as a truncated power or Fourier series, (5.16), (5.17) have the advantage that the expansion coefficients are all of the same order of magnitude, and, hence, will all be determined up to the same order of accuracy. Moreover, the maximum permissible variation in the unknown profiles can be adjusted via the parameter M.

Taking into account the information that the unknown profiles can be represented by (5.16), (5.17) requires a different inversion procedure than the Fourier inversion used in (5.8), (5.9). While keeping the identification of $\hat{\chi}_B(k)$ and $\hat{\sigma}_B(k)$ as specified in (5.6), (5.7), we now obtain the coefficients $\{\chi_m\}$ and $\{\sigma_m\}$ from minimizing the cost functions

$$\begin{aligned} &\int_0^{k_{max}} \left| \sum_{m=0}^{M} \chi_m \hat{\phi}_m(k) - \hat{\chi}_B(k) \right|^2 dk \\ &\qquad + \delta \sum_{m=1}^{M-1} (\chi_{m-1} - 2\chi_m + \chi_{m+1})^2 \\ &+ \delta(2\chi_0 - 3\chi_1 + \chi_3)^2 + \delta(2\chi_M - 3\chi_{M-1} + \chi_{M-3})^2, \end{aligned} \tag{5.19}$$

and

$$\begin{aligned} &\int_0^{k_{max}} \left\{ \frac{k_0^2}{k^2 + k_0^2} \left| \sum_{m=0}^{M} \sigma_m \hat{\phi}_m(k) - \hat{\sigma}_B(k) \right|^2 \right\} dk \\ &\qquad + \delta \sum_{m=1}^{M-1} (\sigma_{m-1} - 2\sigma_m + \sigma_{m+1})^2 \\ &+ \delta(2\sigma_0 - 3\sigma_1 + \sigma_3)^2 + \delta(2\sigma_M - 3\sigma_{M-1} + \sigma_{M-3})^2, \end{aligned} \tag{5.20}$$

where $\hat{\phi}_m(k)$ denotes the spatial Fourier transform of a triangular expansion function $\phi_m(z)$ as defined in Equation (5.18). Computationally, this minimization involves nothing but the least-squares inversion of an overdetermined system of properly normalized linear equations for $(M+1)$ unknown coefficients.

In the cost functions defined above, three aspects require further explanation. In the first place, the weighting function $w(\omega)$ introduced in (4.4) has been chosen in conformity with the error estimations (5.12), (5.13). In (5.20), the parameter k_0 allows adjusting the change-over between a "low-frequency" range, where $w(\omega) = \mathcal{O}(1)$, and a "high-frequency" range, where $w(\omega) = \mathcal{O}(k^{-1})$. In the second place, the number of subintervals in the piecewise-linear expansions (5.16), (5.17) should be chosen such that the additional information about the short-range variation of $\chi(z)$ and $\sigma(z)$ links up with the information about the longer-range variation available from $\hat{\chi}_B(k)$ and $\hat{\sigma}_B(k)$. From that point of view, it seems sensible to take the length of the subintervals approximately equal to half of the wavelength associated

with the maximum value of k for which $\hat{\chi}_B(k)$ and $\hat{\sigma}_B(k)$ are available, i.e. $M \approx k_{max}/\pi$. For an M in that range, however, the local oscillations in the Born-approximation results as observed in Figure 5.1 may pass into an unwanted alternating behavior in the coefficients $\{\chi_m\}$ and $\{\sigma_m\}$. This explains the third new aspect of the cost functions specified in (5.19), (5.20), i.e. the inclusion of the terms proportional to δ. These so-called *regularization terms* can be envisaged as favoring the "most linear" solution in case of ambiguity, with δ being a small nonnegative *regularization parameter* (see also [46, Subsection 5.3.4], [50]).

Some representative numerical results are given in Figure 5.3, which shows results of reconstructing a quadratic susceptibility profile and a quadratic conductivity profile in the Born approximation as well as by the numerical method. Figures 5.3a,b pertain to the case where the regularization terms have been dropped from the cost functions, i.e. $\delta = 0$ in (5.19), (5.20). Clearly, the results obtained by minimizing these cost functions are no better than the Born results. Figures 5.3c,d present the results of repeating the computation with $\delta = 0.001$. Now the results obtained by minimizing (5.19), (5.20) are considerably better. This numerical experiment confirms both the effectiveness of the modified method and the ambiguity in the representations (5.16), (5.17) for $M \approx k_{max}/\pi$.

Finally, it should be remarked that, since the modified method does not affect the low-frequency spectral components of the reconstructed profiles, its range in contrast is the same as that of the closed-form inversion procedure.

5.4 Perturbation approach

The Neumann-series approach described at the beginning of Section 5.2 suggests that it should also be possible to cast the Born inversion procedure proposed in Section 5.1 into the framework of a perturbation approach. Numerical results of such a perturbation approach have not yet been obtained. Nevertheless, its close resemblance to the Born-type iterative approaches that will be discussed in Chapter 6 seems to warrant its inclusion in the present paper.

To arrive at the relevant equations, we augment the series representation

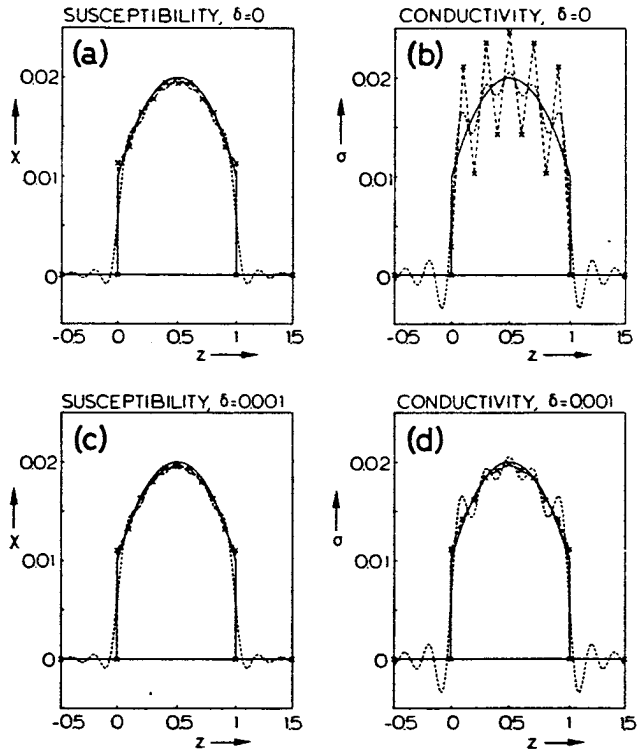

Figure 5.3: Results of the simultaneous Born-type reconstruction of both $\chi(z)$ and $\sigma(z) = 0.02 - 0.04(z - 0.5)^2$ from the reflection coefficients at normal incidence by the methods outlined in Sections 5.1 and 5.3.

(5.14) by similar representations for the unknown profiles, i.e.

$$\chi(z) = \sum_{n=1}^{\infty} \chi^{(n)}(z), \quad \sigma(z) = \sum_{n=1}^{\infty} \sigma^{(n)}(z), \tag{5.21}$$

or, equivalently,

$$C_0(z,s) = \sum_{n=1}^{\infty} C_0^{(n)}(z,s). \tag{5.22}$$

Substituting the expressions (5.14), (5.22) into Equations (3.18), (3.20), and enforcing the equality signs in both equations for each order of magnitude separately then again yield a hierarchy of equations. For the first-order terms $\chi^{(1)}(z)$ and $\sigma^{(1)}(z)$, we end up with the same equations that we found in Section 5.1, i.e. (5.1) with $r_B^{\alpha}(s)$ replaced by $r^{\alpha}(s)$. The higher-order terms can be obtained from

$$\hat{E}_{\alpha}^{(n)}(z,s) = -s^2 \int_0^1 G_0(z,z';s) \sum_{m=0}^{n-1} C_0^{(n-m)}(z',s) \hat{E}_{\alpha}^{(m)}(z',s)\, dz', \tag{5.23}$$

and

$$\int_0^1 C_0^{(n)}(z,s) \hat{E}_{\alpha}^{i}(z,s)\, dz = -\int_0^1 \hat{E}_{\alpha}^{i}(z,s) \sum_{m=1}^{n-1} C_0^{(n-m)}(z,s) \hat{E}_{\alpha}^{(m)}(z,s)\, dz, \tag{5.24}$$

which hold for $n = 1,2,\ldots,\infty$ and for $n = 2,3,\ldots,\infty$, respectively. As remarked in Section 5.2, Equation (5.23) can be resolved by simply evaluating the Fourier-type integral on the right-hand side. Equation (5.24) is of the same form as Equation (5.1), and, hence, can be resolved by either the closed-form procedure described in Section 5.1 or the numerical alternative proposed in Section 5.3.

As in the case of the Neumann-series solution of the direct-scattering problem, it is to be expected that the perturbation approach will suffer from an inherent band limitation. However, the numerical results displayed in Figure 5.3 suggest that this problem can possibly be overcome by taking into account *a priori* information about the short-range variation of the unknown profiles.

Chapter 6

Iterative procedure for larger contrasts

For larger contrasts, we need to invoke the full Born-type iterative scheme proposed in Section 4.2. In that scheme, we start from some initial guess, which should be available from *a priori* information, or be procured from some characteristic features of the known reflected fields. In each iteration step, we then take the reference medium identical to the approximate reconstruction found in the previous step. The essential difference with the perturbation approach proposed in Section 5.4 is that, in the field-computation part of each iteration step, we now compute *exact* solutions to an *approximated* integral equation of the type (3.18) instead of an n-th order *approximate* solution to the *exact* equation.

6.1 The implicit assumptions

As in the case of small contrast, we need to investigate the implicit assumptions formulated in Section 4.3. For a complete justification, we would need closed-form expressions for the unit-amplitude fields $\tilde{E}_\alpha(z,s)$ and $\overline{E}_\alpha(z,s)$ and for the Green's function $\overline{G}(z,z';s)$ for background and reference media of arbitrary inhomogeneity. However, such expressions are not available. Hence, we have to content ourselves with approximate expressions.

For this purpose, we use first-order WKB expressions for the fields $\tilde{E}_\alpha(z,s)$ and $\overline{E}_\alpha(z,s)$ as derived and analyzed in [46, Sections 2.3, 2.4], [48]. For the Green's function $\overline{G}(z,z';s)$, a similar expression can be derived, either by di-

rectly applying the asymptotic solution method described in these references to Equation (3.7), or by substituting the asymptotic expressions obtained for $\overline{E}_a(z,s)$ in (3.8), (3.9) and (3.13). Both procedures lead to the same result.

Numerical experimentation showed that the first-order WKB expressions remain accurate down to surprisingly low frequencies. Consequently, they will at least provide us with a good qualitative description. Moreover, for a homogeneous, lossless slab, the WKB expressions are identical to the actual solutions. Hence, there exists at least one class of reference configurations for which any conclusion from the approximate theory holds rigorously. In particular, this applies to possible ambiguities in the determination of the subsequent approximations to the unknown profile(s). Finally, the WKB expressions are by nature accurate in the high-frequency range, where, according to the analysis given in Chapter 5, most of the difficulties associated with the application of a Born-type approach must be expected.

After a tedious but straightforward calculation, details of which can be found in [46, Subsection 5.2], we find the following approximate correspondence:

$$\begin{aligned} s^{-1}[r^+(s) - \tilde{r}^+(s)] \leftrightarrow \\ -\frac{\tilde{T}^+_{0a}\overline{T}^+_{0a}}{2}\left\{\tilde{D}^+_a(z)\overline{D}^+_a(z)\frac{\epsilon_r(z)-\tilde{\epsilon}_r(z)}{\tilde{N}(z)+\overline{N}(z)}\right. \\ \left. + \int_0^z \tilde{D}^+_a(z')\overline{D}^+_a(z')[\sigma(z')-\tilde{\sigma}(z')]\,dz'\right\}\Big|_{z=z^+(t)}, \end{aligned} \tag{6.1}$$

for $0 < t < \tilde{\tau} + \overline{\tau}$. In (6.1), we have introduced the following quantities:

$$\begin{aligned} N(z) \stackrel{\text{def}}{=} \sqrt{\epsilon_r(z)},\ \ \tau \stackrel{\text{def}}{=} \int_0^1 N(z)\,dz,\ \ T^+_{0a} \stackrel{\text{def}}{=} 2/[N(0)+1], \\ D^+_a(z) \stackrel{\text{def}}{=} \sqrt{N(0)/N(z)}\exp\left[-\int_0^z \sigma(z')/2N(z')\,dz'\right], \end{aligned} \tag{6.2}$$

with the tildes and the bars referring to the background medium and the reference medium, respectively. In (6.2), $N(z)$ denotes the local index of refraction, τ the one-way travel time across the slab, T^+_{0a} the asymptotic transmission factor through the slab interface at $z = 0$ for propagation in the positive z-direction, and $D^+_a(z)$ the attenuation factor for propagation inside the slab from $z' = 0$ to $z' = z$. The point of observation $z^+(t)$ in (6.1)

is the solution of the travel-time equation

$$\int_0^{z^+(t)} [\tilde{N}(z') + \overline{N}(z')]\, dz' = t. \tag{6.3}$$

The correspondence in Equation (6.1) indicates that its right-hand side can be interpreted as an approximation of the difference between the responses of the actual and the background configuration to a step-function pulse incident from $\mathcal{D}_1$. The difference between the impulse responses of these configurations is then approximately equal to the time-derivative of the right-hand side of (6.1), and, hence, is just a linear combination of a distorted version of $d_z[\epsilon_r(z) - \tilde{\epsilon}_r(z)]$ and a distorted version of $[\sigma(z) - \tilde{\sigma}(z)]$. The travel-time equation (6.3) indicates that the time it takes for information about the constitutive parameters at a point inside the slab to show up at $z = z_+ = 0$ is the sum of the travel times in the actual medium from $z = 0$ up to that point, and in the background medium back to $z = 0$.

For $t > \tilde{\tau} + \overline{\tau}$, we find terms that are considerably smaller in magnitude. For incidence from $\mathcal{D}_3$, a similar, independent linear combination can be obtained.

For the Born error $\Delta r_B^\alpha(s)$ defined in (4.3), we find two different estimates. When the reference medium is different from the background medium, we can generalize (5.11) to

$$\Delta r_B^\alpha(i\omega) = \omega \mathcal{O}(\epsilon_r - \tilde{\epsilon}_r)\mathcal{O}(\epsilon_r - \overline{\epsilon}_r), \tag{6.4}$$

for real-valued ω, with $|\ \omega\ | \to \infty$. For the case where both media are identical, a slightly more intricate analysis results in

$$\Delta r_B^\alpha(i\omega) = \Delta r_1^\alpha(i\omega) + \Delta r_2^\alpha(i\omega), \tag{6.5}$$

with

$$\Delta r_1^\alpha(i\omega) = \omega \mathcal{O}[(\epsilon_r - \overline{\epsilon}_r)^2], \tag{6.6}$$

$$\Delta r_2^\alpha(i\omega) = \omega \mathcal{O}(\epsilon_r - \overline{\epsilon}_r)\mathcal{O}(\chi), \tag{6.7}$$

as $|\ \omega\ | \to \infty$. In the time signals corresponding to the Born error, the first term takes effect from $t = 0$, and the second one from $t = 2\overline{\tau}$. The factor of $\mathcal{O}(\chi)$ originates from an asymptotic reflection coefficient at one of the slab's interfaces, and has been included to retain compatibility with the estimate (5.11) as $\chi \to 0$.

These results lead to the following conclusions for the validity of the implicit assumptions, and, hence, for the feasibility of the Born-type iterative scheme:

- Irrespective of the choice of the background medium, the error $\Delta r_B^\alpha(i\omega)$ is of the same order of magnitude as the improvements $\epsilon_r(z) - \bar{\epsilon}_r(z)$ and $\sigma(z) - \bar{\sigma}(z)$ that one would like to obtain. As $\mid \omega \mid \rightarrow \infty$, this error dominates over $r^\alpha(i\omega) - \bar{r}^\alpha(i\omega)$, which is of $\mathcal{O}(\epsilon_r - \bar{\epsilon}_r)$. Hence, a computation neglecting this error can at best yield a band-limited approximation of these improvements.

- In view of this inherent band limitation, it seems best to base the reconstruction procedure only on the terms dominating the reflected fields, i.e. the one approximated in (6.1), and its counterpart for incidence from $\mathcal{D}_3$. As a consequence, we can at best reconstruct a *single* unknown profile from *one-sided* reflection data. In that case the other constitutive parameter must be known. For a unique reconstruction of both profiles, at least *two-sided* reflection data must be available.

- In the calculations leading to the estimates (6.4)–(6.7), it was found that the operator producing $\Delta r_B^\alpha(i\omega)$ from $\epsilon_r(z) - \bar{\epsilon}_r(z)$ and $\sigma(z) - \bar{\sigma}(z)$ becomes more and more independent of $\bar{\epsilon}_r(z)$ and $\bar{\sigma}(z)$ as these approach the actual profiles. Consequently, if the iterative scheme converges, the band limitation in the recovered profiles as well as the rate of convergence will, in general, become constant in the finite stages of the procedure. In particular, this applies to *any* frequency-domain version of the procedure, as well as to time-domain versions where the background medium *differs* from the reference medium.

- The only possible way to free the final result of an iterative reconstruction from the band-limiting effects inherent in the Born-type approximation, therefore, is to avoid the error $\Delta r_2^\alpha(i\omega)$ in (6.5)–(6.7) completely. To this end, we must, in each iteration step, take the background medium *identical* to the reference medium, and consider the time-domain signals corresponding to $r^\alpha(s) - \bar{r}^\alpha(s)$ in the time interval $0 < t < 2\bar{\tau}$ only. In that case, the factor of $\mathcal{O}[(\epsilon_r - \bar{\epsilon}_r)^2]$ may remove the band limitation in the reconstructed profiles as the iterative scheme progresses, provided that we can keep the high-frequency errors within bounds in the initial steps.

- The optimum choice for a weighting function $w(\omega)$ in a frequency-domain error of the type (4.4) is governed by the frequency behavior of the error $\Delta r_B^\alpha(i\omega)$ as well as by the distribution of the profile information over the frequency range. The error $w(\omega) \mid \Delta r_B^\alpha(i\omega) \mid$ must be of the same order of magnitude over the entire frequency range. Moreover, (6.1) indicates that, for high frequencies, $r^\alpha(i\omega)$ mainly depends on a few select properties of the slab. The remaining properties of the slab, which are of interest in the inverse-scattering problem, only influence correction terms of $\mathcal{O}(\omega^{-1})$. Both these observations indicate that $w(\omega)$ must be of $\mathcal{O}(\omega^{-1})$ as $\mid \omega \mid \rightarrow \infty$.

- In order to obtain convergence, we must, at least in the initial iteration steps, supplement the band-limited profile information available through the Born-type approximation with *a priori* information about the short-range variation. Furthermore, the correspondence (6.1) prescribes that any band limitation in the available reflected-field data will give rise to an additional band limitation in the spectral content of the reconstructed profiles that must be compensated for by supplying such *a priori* information throughout the procedure.

Summarizing, only a single version of the Born-type iterative scheme seems capable of reconstructing the unknown slab configuration in full detail. All other versions suffer from an inherent band limitation. From a physical point of view, this seems satisfactory since, according to the travel-time equation (6.3), the version selected is the only one that directly relates the material properties inside the slab to the transient fields at those instants when the relevant reflected waves actually arrive at the slab's interfaces. In this scheme, the configuration is eventually determined from time-domain reflected fields for $0 < t < 2\tau$.

6.2 Numerical implementation

For the case of a vacuum background medium, the Born-type iterative scheme and most of its properties were first found from numerical experimentation. The time-domain case is discussed in [45], and the frequency-domain case in [49]. Both these papers consider the case of a single unknown profile. The simultaneous reconstruction of both profiles from two-sided time-domain

data is described in [46, Section 6.2]. These references contain a detailed account of the implementation, and a series of representative results. In the present discussion, therefore, we restrict ourselves to the implementation and application of the time-domain version with the background medium being identical to the reference medium. To facilitate the comparison with previous applications, we consider the susceptibility $\chi(z)$ rather than the relative permittivity $\epsilon_r(z)$.

In our numerical experiments, the known reflected-field data were generated by applying the marching-on-in-time method as described in [45] and [46, Section 3.3] to compute the response to sine-squared incident pulses of duration T. In some experiments, multiplicative or additive noise was superimposed on the sampled reflected fields thus obtained. In all cases, a high-frequency band limitation was simulated by subjecting the resulting time signals to a low-pass filtering with the cut-off at the first zero in the spectrum of the sine-squared pulse, i.e. at $\mid \omega \mid = \omega_{max} = 4\pi/T$.

The iteration procedure as such runs along the same lines as the numerical inversion procedure discussed in Section 5.3. Let us consider the general case where both profiles are unknown. These unknown profiles are again approximated by the piecewise-linear expansions specified in (5.16)–(5.18). Substituting these expressions and (2.11) in (4.2) results in the approximate linear equations

$$E^r_\alpha(z_\alpha, i\omega) - F(i\omega)\overline{E}^r_\alpha(z_\alpha, i\omega) = \\ -\frac{1}{2}\left\{ i\omega \sum_{m=0}^{M} \Delta\chi_m E^\alpha_m(i\omega) + \sum_{m=0}^{M} \Delta\sigma_m E^\alpha_m(i\omega) \right\}, \tag{6.8}$$

with $\alpha = \pm$, where

$$E^\alpha_m(i\omega) \stackrel{\text{def}}{=} F(i\omega) \int_0^1 \phi_m(z)\overline{E}_\alpha(z, i\omega)^2\, dz, \tag{6.9}$$

and where $\Delta\chi_m \stackrel{\text{def}}{=} \chi_m - \overline{\chi}_m$ and $\Delta\sigma_m \stackrel{\text{def}}{=} \sigma_m - \overline{\sigma}_m$. In our computations, the unit-amplitude reference fields $\overline{E}_\alpha(z, s)$ were determined by applying the Runge-Kutta-Verner integration procedure discussed in [46, Subsection 2.4.2], [48] and [49] to the system of first-order differential equations (3.4), (3.5). The integrals in (6.9) were then evaluated with the aid of a repeated trapezoidal rule.

Applying a fast Fourier algorithm to the discretized equations (6.8) results in a low-pass filtered version of their time-domain counterparts

$$\mathcal{E}^{\tau}_{\alpha}(z_{\alpha},t)-\overline{\mathcal{E}}^{\tau}_{\alpha}(z_{\alpha},t)=-\frac{1}{2}\sum_{m=0}^{M}\Delta\chi_m\partial_t\mathcal{E}^{\alpha}_{m}(t)-\frac{1}{2}\sum_{m=0}^{M}\Delta\sigma_m\mathcal{E}^{\alpha}_{m}(t), \qquad (6.10)$$

where $\overline{\mathcal{E}}^{\tau}_{\alpha}(z,t)$ denotes a time-domain reflected field that would be excited by the sine-squared pulse in the reference medium.

Having obtained these approximate time-domain equations, we determine the *profile updates* $\Delta\chi(z)$ and $\Delta\sigma(z)$ by determining those sets of coefficients $\{\Delta\chi_m\}$ and $\{\Delta\sigma_m\}$ that minimize the squared error

$$\begin{aligned}\sum_{\alpha}\int_{T/2}^{2\tau+T/2}\Bigg\{&\mathcal{E}^{\tau}_{\alpha}(z_{\alpha},t)-\overline{\mathcal{E}}^{\tau}_{\alpha}(z_{\alpha},t)+\frac{1}{2}\sum_{m=0}^{M}\Delta\chi_m\partial_t\mathcal{E}^{\alpha}_{m}(t)\\&+\frac{1}{2}\sum_{m=0}^{M}\Delta\sigma_m\mathcal{E}^{\alpha}_{m}(t)\Bigg\}^{2}dt\\&+\delta\sum_{m=1}^{M-1}[\Delta\chi_{m-1}-2\Delta\chi_m+\Delta\chi_{m+1}]^2\\&+\delta\sum_{m=1}^{M-1}[\Delta\sigma_{m-1}-2\Delta\sigma_m+\Delta\sigma_{m+1}]^2.\end{aligned} \qquad (6.11)$$

As in the case of the cost functions (5.19), (5.20), this minimization amounts to the least-squares inversion of an overdetermined system of properly normalized linear equations, now for $(2M+2)$ unknown coefficients.

In choosing the integration interval in (6.11), the finite duration T of the sine-squared pulse was taken into account. The parameter M, which represents the number of cells in the piecewise-linear expansions (5.16), (5.17), should be adjusted to the cut-off frequency in the low-pass filtering as well as to the two-way travel time 2τ. When the permittivity is discontinuous at at least one end of the slab, this travel time can be estimated from the arrival times of the waves directly reflected at that interface. According to Shannon's theorem, the shortest sampling period for which samples of the band-limited time signals are independent is $\Delta t=\pi/\omega_{max}=T/4$. Hence, we can at most recover $M\approx 8\tau/T$ independent parameters for each unknown profile. In view of the distortion effects observed in Equations (6.1) and (6.3), we choose M at least a factor of 2 larger to ensure that the maximum

amount of profile information is drawn from the reflected fields. As argued in Section 5.3, we can rely on the regularization terms to eliminate any ambiguity due to this oversampling, and, in the first few iteration steps, due to the band limitations inherent in the Born-type approach. Compared with the cost functions specified in (5.19), (5.20), the "boundary terms" appearing on the last lines of (5.19), (5.20) have been left out. This leads to a better reconstruction, without affecting the convergence.

For the case of a single unknown contrast, we follow the same approach as outlined above, with the exceptions that the summation in (6.11) now runs over $\alpha = +$ only, and that one of the sets of coefficients $\{\Delta\chi_m\}$ and $\{\Delta\sigma_m\}$ vanishes in Equations (6.8)–(6.11).

Finally, it should be remarked that the implementation above is not the fastest one that can be imagined. In particular, the application of the Runge-Kutta-Verner integration may be overly time consuming. However, by choosing different algorithms for generating the "known" and the "reference" fields, we have automatically avoided the possibility of the solution of the inverse-scattering problem being biased by numerical errors made in solving the underlying direct-scattering problem.

6.3 Numerical results

In order to obtain insight into the potentialities of the computational scheme described in Sections 6.1, 6.2, we carried out a number of numerical experiments. In particular, we attempted to reconstruct some profiles that were previously considered elsewhere in the literature.

Figures 6.1–6.3 present results of reconstructing the unknown susceptibility profiles of lossless slabs that were previously analyzed in [45]. In Figures 6.1 and 6.2, results are given for the same sine-squared susceptibility profile as in Figure 5 of [45]. Clearly the present approach leads to a better reconstruction, even for a considerably longer incident-pulse duration ($T = 0.7$ instead of $T = 0.15$). Further, it is observed from Figure 6.2 that an evaluation of the root-mean-quare error in the reflected field provides a good indication of the progress of the iterative procedure.

In Figure 6.3, we consider two discontinuous slab profiles. For such profiles, we obviously miss some of the high-frequency information needed to reconstruct them in full detail. In [46], this necessitated the use of a short

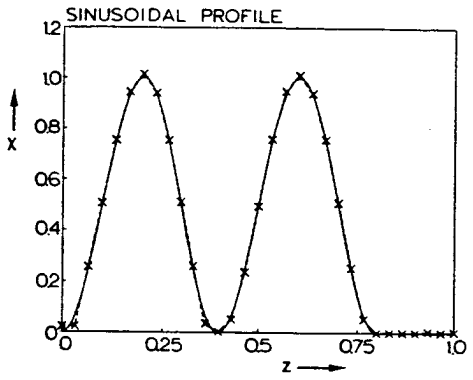

Figure 6.1: Actual profile $\chi(z) = \sin^2(2.5\pi z) \times U(0.8 - z)$ obtained after six iteration steps of the Born-type iterative procedure for $\sigma(z) = 0$, $M = 30$, $T = 0.7$, $\delta = 5 \times 10^{-4}$ and initial estimate $\overline{\chi}(z) = 0.5$.

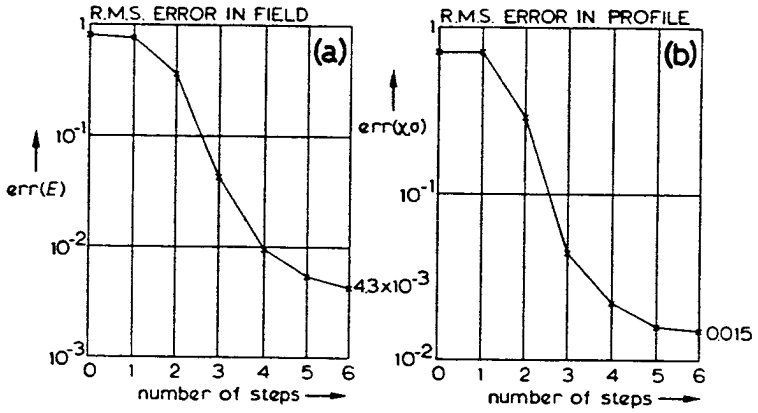

Figure 6.2: Root-mean-square errors in $\overline{\mathcal{E}}_+^r(0,t)$ and $\overline{\chi}(z)$ as a function of the number of iteration steps for the computation leading to Figure 6.1.

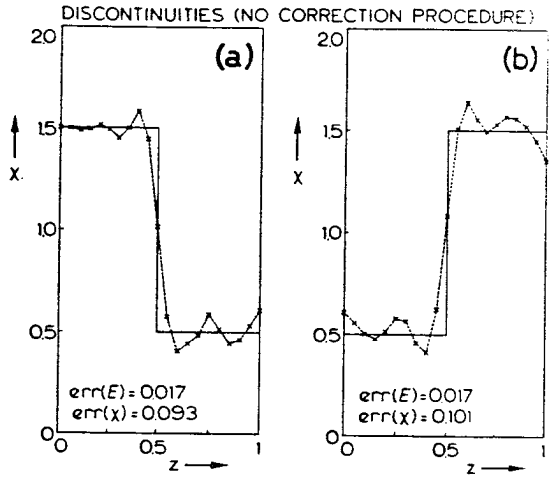

Figure 6.3: Actual susceptibility profiles $\chi(z) = 1.5 - U(z - 0.5)$ and $\chi(z) = 0.5 + U(z - 0.5)$ compared with the reconstructions obtained after ten iteration steps of the improved Born-type procedure for $\sigma(z) = 0$, $M = 20$, $T = 1$, $\delta = 10^{-3}$ and initial estimate $\overline{\chi}(z) = 1.0$.

pulse ($T = 0.3$), as well as the application of a discontinuity correction. In Figure 6.3, we have found a "filtered" version of the unknown profiles by directly applying our modified Born-type procedure to the reflected field caused by a pulse of duration $T = 1$. The root-mean-square field errors listed in this figure indicate that, from the band-limited field information available, we can hardly expect to obtain a more detailed reconstruction.

The ultimate test of our improved Born-type scheme was the reconstruction of a piecewise-homogeneous, lossy three layer medium as considered in [9]. Figure 6.4 shows the results obtained in every second iteration step. For the unknown susceptibility profile, we obtain a reconstruction of at least the same quality as we obtained in Figure 6.3. Apparently, the imperfections in the recovered susceptibility profile do degrade the reconstruction of the conductivity profile. This was confirmed by repeating the computation of Figure 6.4 for the same conductivity profile and a continuous susceptibility profile. Nevertheless, we do obtain the correct trend for the conductivity profile as well. Moreover, the size of the root-mean-square field errors listed in Figure 6.4 indicates that the reflection coefficients $r^a(i\omega)$ of the exact configuration and those of its reconstruction given in Figures 6.4e,f may be

almost indistinguishable over the frequency range excited by the incident pulse. This would mean that a better reconstruction may be obtained from the reflected fields corresponding to a shorter pulse. We will come back to this in Section 7.3.

From the results displayed in Figure 6.4, it is also observed that, in the first few iteration steps, mainly the average behavior of the unknown profiles is recovered. In subsequent steps, we obtain a more detailed impression of their local behavior. This detail, in particular, appears to be missing from the frequency-domain reconstructions presented in [9]. This observation agrees well with the conclusion reached in Section 6.1 that, only in the present scheme, the band limitation inherent in the Born-type approximation is gradually removed as the iterative procedure progresses.

For the reconstruction of a lossless slab with the same susceptibility profile as considered in Figure 6.4 from a comparable amount of reflected-field information, the result a frequency domain Born-type reconstruction with a vacuum background medium was presented in Figure 5 of [49]. Both the result given in Figure 6.4e and one obtained for the corresponding lossless case turn out to be considerably better.

Similar numerical experiments were also performed for cases where multiplicative or additive noise was superimposed on the known reflected-field data. We found that superimposing up to 10% multiplicative noise or up to 1% additive noise hardly affects the reconstructions obtained. Possibly, this can be explained from the fact that a significant part of this noise is removed in the low-pass filtering.

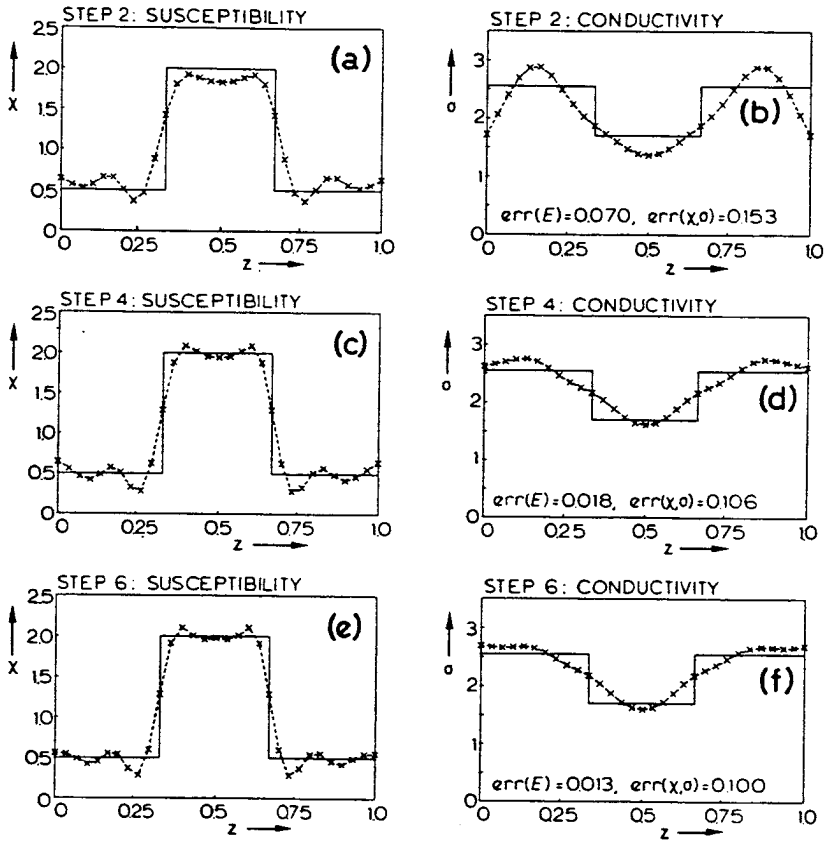

Figure 6.4: Actual three-layer profiles and reconstructions obtained with the improved Born-type procedure with $M = 30$, $\delta = 10^{-4}$, and initial estimates $\overline{\chi}(z) = 1$ and $\overline{\sigma}(z) = 0$.

Chapter 7

Validation of the results

Although the numerical results presented in Section 6.3 seem fairly conclusive, the use of the WKB expressions in Section 6.1 still leaves room for some doubt. Hence, it seems appropriate to obtain an independent confirmation of the validity of our analysis. In this chapter, we review three ways to achieve this.

7.1 Approximate inversion procedure for lossless slabs

For the case of a lossless slab, additional confidence in the WKB results (6.1) and (6.6) can be gained by using them to generate an approximate inversion procedure. Taking in (6.1) the background medium identical to the reference medium, we can interpret its right-hand side as the first-order term in a Taylor expansion of the unit-step response $\mathcal{E}_+^r(0,t)$ around the corresponding reference solution $\overline{\mathcal{E}}_+^r(0,t)$ in terms of the susceptibility difference $\chi(z^+(t)) - \overline{\chi}(z^+(t))$. The coefficient of $\chi(z^+(t)) - \overline{\chi}(z^+(t))$ can then be identified as a "profile derivative" of the reflected field $\mathcal{E}_+^r(0,t)$. A closed-form integration of this derivative from $\chi = \chi(0)$ to $\chi = \chi(z^+(t))$ leads to a closed-form relation between $\mathcal{E}_+^r(0,t)$ and $\chi(z^+(t))$, which, in turn, can be inverted in closed form. We then end up with level and position corrections for the Born results discussed in Section 5.1. These corrections are similar to those found in [19], [43] and [44]. Since we start the χ-integration from a homogeneous, lossless half-space with $\chi(z) = \chi(0)$, this procedure will be most accurate for a small variation in the value of $\chi(z)$.

For the precise expressions, the reader is referred to [46, Subsection 5.4.2].

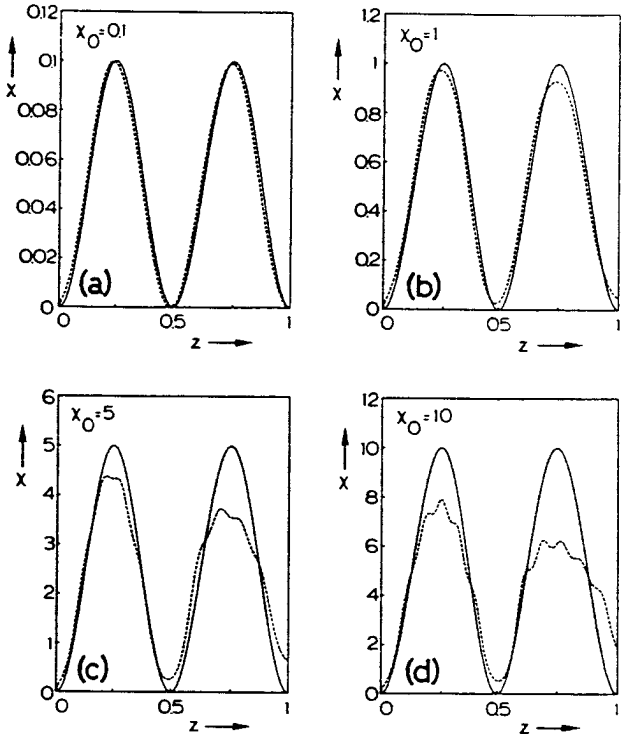

Figure 7.1: Results of the WKB version of the corrected Born approximation (dashed lines) compared with the actual susceptibility profiles (solid lines) $\chi(z) = \chi_0 \sin^2(2\pi z)$ for increasing contrast.

Here, we confine ourselves to showing the representative results given in Figure 7.1. Clearly, the approximate inversion method is succesful even for a relatively large variation in the value of $\chi(z)$. Hence, the underlying WKB approximations should certainly be applicable in the context of Section 6.1, where the reference configuration is assumed to be close to the actual configuration.

7.2 Optimization approach

An alternative way to resolve the inverse-profiling problem discussed in this paper is to minimize a cost function of the form

$$\sum_{\alpha} \int_0^{\infty} \left\{ \mathcal{E}_{\alpha}^{r}(z_{\alpha},t) - \overline{\mathcal{E}}_{\alpha}^{r}(z_{\alpha},t) \right\}^2 dt + \delta \sum_{m=1}^{M-1} [\chi_{m-1} - 2\chi_m + \chi_{m+1}]^2 + \delta \sum_{m=1}^{M-1} [\sigma_{m-1} - 2\sigma_m + \sigma_{m+1}]^2 \tag{7.1}$$

as a function of the parameters $\{\chi_m\}$ and/or $\{\sigma_m\}$ with the aid of a *nonlinear optimization method.* In (7.1), the summation runs over one or both of the labels $\alpha = \pm$, according to whether one or both of the contitutive parameters $\chi(z)$ and $\sigma(z)$ are unknown. The reflected fields $\overline{\mathcal{E}}_{\alpha}^{r}(z_{\alpha},t)$ pertain to some *trial medium*, in which the unknown profile(s) are given by the piecewise-linear expansions (5.16) and/or (5.17). The main advantage of the optimization approach is that we can now use *all* the reflected-field information in the time interval $0 < t < \infty$. In addition, we can relate the reflected field(s) $\mathcal{E}_{\alpha}^{r}(z_{\alpha},t)$ to the unknown profile(s) via the integral relation (3.20) without experiencing an inherent band limitation.

An approach of this type was previously proposed by Lesselier [32], [33]. The fundamental improvement in our version is that we purposely choose the expansion of the unknown profile(s) in conformity with the amount of information available from the known reflected field(s). We experimented with both quasi-Newton and conjugate-gradient procedures available from standard mathematical subroutine libraries. The most efficient reconstruction procedure was obtained by combining a conjugate-gradient method with an independent evaluation of the "gradient" (the vector containing the partial derivatives of the cost function with respect to the unknown profile parameters) as outlined in [32], [33]. Even for this procedure, however, a typical computation took an effort equivalent to tens of iteration steps in the Born-type procedure.

The fact that a conjugate-gradient method converges faster than quasi-Newton methods provides yet another confirmation of the applicability of the approximate correspondence (6.1): only if the cost function varies almost

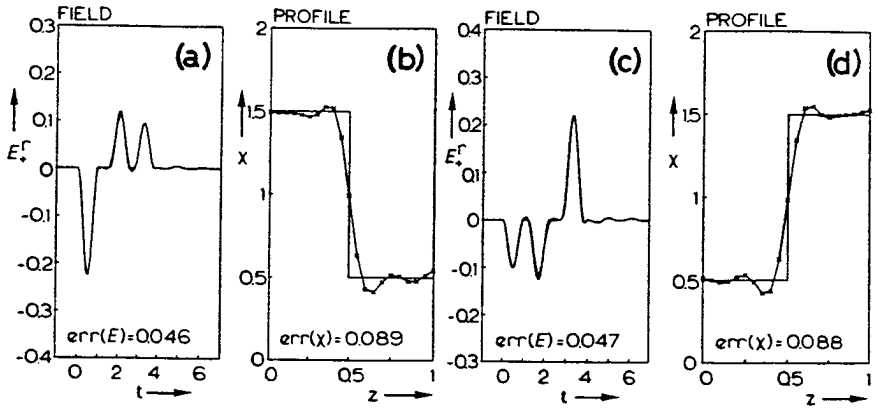

Figure 7.2: Results of reconstructing the susceptibility profiles specified in Figure 6.3 for $\sigma(z) = 0$, $M = 20$, $T = 1$ and initial estimate $\overline{\chi}(z) = 1$ by nonlinear optimization.

quadratically with the parameters $\{\chi_m\}$ and $\{\sigma_m\}$ will a conjugate-gradient method be more efficient than a quasi-Newton method (see e.g. [14]).

As an illustration, we present in Figure 7.2 results of reconstructing the same two discontinuous susceptibility profiles that we considered previously in Figure 6.3. In this figure, we show the actual and the reconstructed configurations, as well as the corresponding reflected fields. Both from Figures 7.2b,d and from the r.m.s. errors listed, it is observed that the reconstructed profiles are of approximately the same quality as the ones displayed in Figure 6.3. The increase in the r.m.s. error for the reflected fields can be explained from the fact that we now have used unfiltered fields over the entire interval $0 < t < \infty$. The deviations between the fields given in Figures 7.2a,c indicate that, possibly, a slightly better reconstruction can be obtained by making the piecewise-linear expansions (5.16), (5.17) more flexible near the discontinuities.

7.3 A Prony-type method

Now that we have solved the inverse-scattering problem, we have two different ways of finding the natural frequencies of a slab configuration from time-domain reflected-field data. In the first place, we can follow the indirect route

Table 7.1: Comparison of the actual natural frequencies of the slab configuration specified in Figure 6.4 with the ones recovered from the time-domain reflected fields excited by a sine-squared incident pulse with $T = 0.7$.

Actual natural frequency	*Approximation from profile reconstruction*	*Approximation from Prony-type method*
-4.819	-4.962	
-4.422	-4.659	-4.569
-2.635	-2.490	-2.631
-2.186+i3.195	-2.151+i3.144	-2.186+i3.195
-1.824+i6.145	-1.795+i6.097	-1.818+i6.142
-2.224+i9.110	-2.153+i9.092	-2.195+i9.084
-2.588+i10.960	-2.553+i10.973	-2.471+i11.049
-2.143+i12.851	-2.180+i12.818	-2.162+i12.889
-1.943+i15.797	-1.814+i15.510	-1.628+i15.822

of first reconstructing the configuration with the aid of the Born-type iterative procedure. Subsequently, we can then compute the natural frequencies of the reconstructed configuration as explained in [48]. In the second place, we can resample the filtered time signals mentioned in Section 6.2 with a suitably chosen sampling period, and directly apply Prony's method [35], [46, Section 4.3] to the resampled signal.

By comparing the two sets of results thus obtained with each other and with the actual natural freqencies, we can resolve two issues at once. In the first place, we can verify our conclusion that reconstructed configurations as shown in Figures 6.3 and 6.4e,f have the same reflection coefficients as the actual configuration over the real-frequency range excited. If this conclusion is correct, we should observe good agreement between the natural frequencies of the reconstructed configurations whose imaginary parts lie in that range and their actual counterparts. In the second place, we can decide whether the piecewise-linear expansions employed are flexible enough. If the deviation between the indirectly obtained natural frequencies and those obtained otherwise increases considerably with their increasing imaginary parts, it may be necessary to choose a larger number of subintervals, i.e. a larger M.

In Table 7.1, results are presented of determining the natural frequencies as proposed above for the lossy three-layer slab specified in Figure 6.4. With

the obvious exception of the real part of the natural frequency nearest to the cut-off frequency of the low-pass filtering, the Prony results turn out to be slightly better than the results obtained indirectly by determining the natural frequencies of the reconstructed configuration given in Figures 6.4e,f. This suggests that a slight improvement of that reconstruction should, in principle, be possible. This would be in agreement with the rather large field error remaining in the final iteration step. In view of the relatively small reduction of the field error achieved in steps 5 and 6, however, it does not seem sensible to try and obtain this improvement by carrying out more iteration steps.

From Table 7.1, it is also observed that Prony's algorithm is not able to distinguish between the two poles located close together at the far end of the negative real s-axis. Instead, only a single pole with a residue twice as large is recovered. This can be explained from the feature that the natural frequency of a more rapidly decaying exponential is obtained with less accuracy. On the other hand, especially the natural frequencies nearest to the origin of the complex s-plane are recovered well by the Prony-type method. Hence, comparing these frequencies with those obtained indirectly via profile reconstruction may indeed provide an additional way of judging the quality of the reconstructed profiles.

Chapter 8

Conclusions

With the analysis presented in this paper, we have established a more rigorous theoretical foundation for the Born-type reconstruction of material parameters of an inhomogeneous, lossy dielectric slab. In our analysis, two key points are equally important. In the first place, the Born-approximated equations for the unknown profiles should be uniquely solvable, at least within some limitations. In the second place, the Born error made in formulating these equations should be small enough for the solutions obtained to be better approximations than the estimates previously available.

For the configuration at hand, only a single version of the Born-type iterative scheme exists that meets both these requirements, and, hence, may lead to a fully detailed determination of the unknown constitutive parameters. When sufficient reflected-field information is available, this version of the Born-type iterative scheme appears to be as powerful as any of the "exact" approaches involving a Liouville transformation. Moreover, by avoiding that transformation, we have kept open the possibility of using more realistic, incomplete reflected-field data, and, probably, of generalizing the approach to more complicated geometries.

The conclusions from our closed-form analysis have been verified in two ways. First, we have implemented the Born-type scheme numerically, taking into account the consequences of the closed-form analysis. The quality of the profile reconstructions obtained exceeds the quality attained previously with other iterative procedures considerably. Second, we have independently validated our analytical and numerical results by invoking optimization and Prony-type techniques.

Finally, it is recommended that any generalization of our approach to more complicated geometries starts off with an analysis of the case of small contrast, as performed in Chapter 5. For that case, the Born inversion has already been analyzed and implemented in the context of a variety of practical imaging techniques (see [29]). In fact, the success of this application and the limited availability of scattered-field data indicate that it may be worthwhile to enhance the low-contrast results with the aid of a perturbation approach as proposed in Section 5.4, before tackling the more involved implementation of a full Born-type iterative approach.

Acknowledgments

The research described in this paper was carried out at the Laboratory of Electromagnetic Research of the Delft University of Technology, and has benefited considerably from many helpful discussions with Professor Hans Blok. This paper was written while the author was on leave at the University of Colorado at Boulder, with the financial support of the Netherlands Organization for the Advancement of Pure Research (Z.W.O). The author gratefully acknowledges this support, and the hospitality received from the members of the Electromagnetics Laboratory at Boulder. In particular, he would like to thank Professor Edward F. Kuester, both for his hospitality and for reacquainting him with the perturbation approach.

[33] D. Lesselier, *Diagnostic optimal de la lame inhomogène en régime temporel. Applications à l'électromagnétisme et à l'acoustique*, Ph. D. Thesis, l'Université Pierre et Marie Curie, Paris (1982).

[34] J.M. Mendel and F. Habibi-Ashrafi, "A survey of approaches to solving inverse problems for lossless layered media systems", *IEEE Transactions Geoscience Remote Sensing 18*, 320–330 (1980)

[35] E.K. Miller, "Natural mode methods in frequency and time domain analysis". In: *Theoretical methods for determining the interaction of electromagnetic waves with structures*, J.K. Skwyrzinski (Ed.), Sijthoff and Noordhoff, Alphen aan den Rijn, The Netherlands (1981), 173–212.

[36] M. Mostafavi and R. Mittra, "Remote probing of inhomogeneous media using parameter optimization techniques", *Radio Science 7*, 1105–1111 (1972).

[37] R.G. Newton, "Inverse scattering. I. One dimension", *J. Math. Phys. 21*, 493–505 (1980).

[38] A. Roger, *Problèmes inverses de diffraction en électromagnétisme. Théorie, traitement numérique, et applications à l'optique*, Ph.D. Thesis, l'Université d'Aix-Marseille III, Marseille (1981).

[39] A. Roger, D. Maystre and M. Cadilhac, "On a problem of inverse scattering in optics: the dielectric inhomogeneous medium", *J. Optics 9*, 83–90 (1978).

[40] P.C. Sabatier, "Theoretical considerations for inverse scattering", *Radio Science 18*, 1–18 (1983).

[41] T.K. Sarkar, D.D. Weiner and V.K. Jain, "Some mathematical considerations in dealing with the inverse problem", *IEEE Transactions Antennas Propagat. 29*, 373–379 (1981).

[42] D.H. Schaubert and R. Mittra, "A spectral domain method for remotely probing stratified media", *IEEE Transactions Antennas Propagat. 25*, 261–265 (1977).

[43] W. Tabbara, *Étude de problèmes de diffraction inverse électromagnétique par analyse multifréquentielle des champs diffractés*, Ph.D. Thesis, l'Université Pierre et Marie Curie, Paris (1976).

[44] W. Tabbara, "Reconstruction of permittivity profiles from a spectral analysis of the reflection coefficient", *IEEE Transactions Antennas Propagat. 27*, 241–244 (1979).

[45] A.G. Tijhuis, "Iterative determination of permittivity and conductivity profiles of a dielectric slab in the time domain", *IEEE Trans. Antennas Propagat. 29*, 239–245 (1981).

[46] A.G. Tijhuis, *Electromagnetic inverse profiling: theory and numerical implementation*, VNU Science Press, Utrecht, The Netherlands (1987).

[47] A.G. Tijhuis and H. Blok, "SEM approach to the transient scattering by an inhomogeneous, lossy dielectric slab; Part 1: the homogeneous case", *Wave Motion 6*, 61–78 (1984).

[48] A.G. Tijhuis and H. Blok, "SEM approach to the transient scattering by an inhomogeneous, lossy dielectric slab; Part 2: the inhomogeneous case", *Wave Motion 6*, 167–182 (1984).

[49] A.G. Tijhuis and C. van der Worm, "Iterative approach to the frequency-domain solution of the inverse-scattering problem for an inhomogeneous, lossy dielectric slab", *IEEE Transactions Antennas Propagat. 32*, 711–716 (1984).

[50] A.N. Tikhonov and V.Y. Arsenin, *Solution of ill-posed problems*, V.H. Winston and Sons, Washington D.C. (1977), Chapters II, III.

[51] E.C. Titchmarsh, *The theory of functions*, 2nd ed., Oxford University Press, New York (1950), Chap. 13.

[52] F.G. Tricomi, *Integral equations*, Dover Publications, New York (1985), 49–55.

[53] T. Uno and S. Adachi, "Electromagnetic inverse scattering for one-dimensional inhomogeneous layered media", *Proceedings of the International Symposium on Antennas and Propagation, Kyoto, August 20-22*, 887–890 (1985).

[54] V.H. Weston, "On the inverse problem for a hyperbolic dispersive partial differential equation", *J. Math. Phys. 13*, 1952–1956 (1972).

[55] V.H. Weston, "On inverse scattering", *J. Math. Phys. 15*, 209–213 (1974).

[56] V.H. Weston and R.J. Krueger, "On the inverse scattering problem for a hyperbolic dispersive partial differential equation. II", *J. Math. Phys. 14*, 406–408 (1972).